

COMPUTER SIMULATIONS OF MOLECULAR STICKING ON AMORPHOUS ICE

by

VIJAY KUMAR VEERAGHATTAM

(Under the direction of Steven P. Lewis and Phillip C. Stancil)

Using classical molecular dynamics, we have simulated the sticking and scattering process of atomic and molecular hydrogen on an amorphous ice surface to predict their sticking probabilities. A wide range of initial kinetic energies of the incident hydrogen atom and molecule and two different ice surface temperatures were used to investigate this fundamental process in interstellar chemistry. In this dissertation, we report the sticking probability of atomic hydrogen and H₂ molecule as a function of incident kinetic energy. The sticking coefficients as a function of gas temperature and substrate temperature are calculated, which can be used in astrophysical models. These results are compared to previous theoretical and experimental studies which have reported a wide range in the sticking coefficients.

INDEX WORDS: dust, extinction - abundances, molecular processes

COMPUTER SIMULATIONS OF MOLECULAR STICKING ON AMORPHOUS ICE

by

VIJAY KUMAR VEERAGHATTAM

M.S., Utkal University, India, 2004

M.Tech., University of Hyderabad, India, 2006

A Dissertation Submitted to the Graduate Faculty
of The University of Georgia in Partial Fulfillment

of the

Requirements for the Degree

DOCTOR OF PHILOSOPHY

ATHENS, GEORGIA

2014

©2014

Vijay Kumar Veeraghattam

All Rights Reserved

COMPUTER SIMULATIONS OF MOLECULAR STICKING ON AMORPHOUS ICE

by

VIJAY KUMAR VEERAGHATTAM

Approved:

Major Professors: Steven P. Lewis
Phillip C. Stancil

Committee: David P. Landau
Inseok Song

Electronic Version Approved:

Julie Coffield
Interim Dean of the Graduate School
The University of Georgia
August 2014

Dedicated to my friends and teachers

Acknowledgments

It has been a great privilege to work with Prof. Steven P. Lewis and Prof. Phillip C. Stancil. Their enduring patience, unwavering support, and constant encouragement have made this journey a worthwhile learning experience. I am immensely grateful for this opportunity to learn from these two prolific researchers and outstanding teachers. No words can truly express my gratitude towards them, and I am truly thankful for being one of their doctoral student.

I would like to take this opportunity to thank the founding director of the Center for Simulational Physics, a distinguished Professor and an eminent researcher, Prof. David P. Landau. I would not have heard of Athens or the University of Georgia if not for his work and fame. The simulation techniques I learned in his classes are valuable tools which I will continue to use in my research work. Thank you Dr. Landau for creating the opportunities and a center to work in this area of physics.

A lot of people helped and supported me on this path. Their belief in my abilities has helped me persist through graduate school, and I am really lucky to have some amazing friends, mentors, parents and siblings. Thank you all.

Contents

Acknowledgments	iv
1 Background	2
1.1 Interstellar Medium	2
1.2 Neutral Atomic Gas : Hydrogen (H I)	5
1.3 Molecular Gas : H ₂	6
1.4 Interstellar Dust	7
1.5 Interstellar Molecules	8
1.6 Gas-Phase Chemical Reactions	10
1.7 Grain-Surface Chemistry	12
1.8 Sticking and H ₂ formation	13
2 Molecular Dynamics Simulations	17
2.1 Intoduction	17
2.2 Interaction Potentials	18
2.3 MD Algorithm	21
2.4 Time Integration Algorithms	23
2.5 Constant-temperature MD	25
2.6 Amorphous Solid Water Simulation	26

3	Sticking of Atomic Hydrogen	31
3.1	Introduction	31
3.2	Methodology	34
3.3	Results	38
3.4	Discussion	42
3.5	Conclusion	48
4	Sticking of Molecular Hydrogen	49
4.1	Introduction	49
4.2	Computational Method	52
4.3	Results and Discussion	55
4.4	Conclusion	61
5	Conclusion	62
5.1	Summary	62
5.2	Future Work	64
	Bibliography	65

List of Figures

1.1	Eley-Rideal Mechanism (Eley , 1941)	14
1.2	Langmuir-Hinselwood Mechanism (Hinshelwood, 1930; Langmuir, 1922) . . .	14
1.3	Harris-Kasemo Mechanism (Harris & Kasimo, 1981)	15
1.4	Sticking and scattering of an atom on a surface.	15
2.1	Water molecule in a TIP4P model (Jorgenson, 1982). The positive charges are on the H atoms and negative charge is displaced by 0.15 Å from the O atom. The O–H bond distance is 0.9572 Å and the H–O–H angle is 104.52°	27
2.2	Cubic simulation box of dimensions 40 Å × 40 Å × 40 Å with the slab dimensions 40 Å × 40 Å × 20 Å . Periodic boundary conditions are applied only in x and y directions and removed in the z direction once the slab has been simulated.	28
2.3	A view of the simulated amorphous water ice slab at 10 K. Red and grey balls represent oxygen and hydrogen atoms, respectively.	29
3.1	Sticking probability vs. incident kinetic energy (in K) of H on amorphous water ice at 10 K, compared to the simulations of Zhang et al. (1991), Masuda et al. (1998), and Al-Halabi & van Dishoeck (2007). Results on crystalline ice from Al-Halabi et al. (2002) are shown for comparison.	39

3.2	Sticking probability of H on amorphous water ice at 70 K, compared to the simulations of Masuda et al. (1998) and Al-Halabi et al. (2002). Note, the results for Al-Halabi et al. (2002) are for crystalline ice.	41
3.3	Sticking probability as a function of incident angle for three different incident energies. The temperature of the amorphous ice substrate is held at 10 K and normal incidence angle corresponds to 90°	43
3.4	Predicted sticking coefficient $S(T)$ of H on 10 K amorphous water ice from the present study compared to the quantum model by Hollenbach & Salpeter (1970) and the experiments of Manico et al. (2001) and Watanabe et al. (2010). Note that the experiments measured $\eta S(T)$ and assume a recombination efficiency, η , of 100%. Also plotted is a $T^{-1/2}$ dependence, normalized to 1 at $T = 10$ K. Fit of current results using Equation (3.3) with $\gamma = (244 \text{ K})/T$	44
3.5	Sticking coefficient $S(T)$ of H on 70 K amorphous water ice and fit using Equation (3.3) with $\gamma = (244 \text{ K})/T$ and a prefactor of 0.51. This is compared to $T^{-1/2}$ normalized to 1 at 10K.	46
4.1	Sticking probability vs. incident kinetic energy (in K) of H_2 initially in its ground rovibrational level ($v = 0, J = 0$) on amorphous water ice at 10 K.	56
4.2	Predicted sticking coefficient $S(T)$ of H_2 on 10 K amorphous water ice from the present study compared to the semi-quantum model by Hollenbach & Salpeter (1970) for the two values of the parameter Ω , where $\Omega^2 = 1$ for Lamberts law and $\Omega^2 = 2$ for isotropic scattering. The value of $\Omega^2 = 1$ is typically adopted. Comparision is also made to the quantum mechanical model of Leitch-Devlin & Williams (1985) available only for ice surfaces of 3 and 100 K.	58

4.3 Effective sticking probability as a function of H₂ beam kinetic energy (K) on amorphous water ice at 10 K. The computed sticking probability has been averaged over the experimental beam velocity spread for comparison to the experiment of Matar et al. (2010). The angle of incidence is fixed at 62° from the normal. 60

List of Tables

1.1	Phases of the interstellar medium (Tielens, 2005)	4
1.2	List of molecules detected in the Interstellar Medium and Circumstellar Shells (Müller et al., 2005). http://www.astro.uni-koeln.de/cdms/molecules	9
3.1	Parameters for the H-H ₂ O interaction potential (Zhang et al., 1991).	37
4.1	Parameters for the H ₂ -H ₂ O interaction potential (Zhang & Buch, 1992).	54
5.1	Fit parameters for the Hollenbach & Salpeter (1970) model	63

“Hydrogen is a light, odorless gas, which, given enough time, turns into people.”

–*Edward R. Harrison* (Cosmology: The Science of the Universe)

Chapter 1

Background

1.1 Interstellar Medium

The vast expanse of space in-between the stars, with a very low density of matter, primarily hydrogen, helium, and a few heavy elements, constitutes the interstellar medium (ISM). Stars are separated by an average distance of 1.5 pc¹, and beyond the heliosphere of a star ($\sim 10^2$ AU), the intermediate space between two stars was historically assumed to be empty. This viewpoint has changed in the last 100 years, as astronomers keep observing an increasing number of atoms, molecules and dust in the ISM. This interstellar space is both the graveyard and the cradle of cosmic material. Matter ejected by stars and supernovae explosions, including atomic and molecular hydrogen, ions, carbonate and silica grains are eventually recycled in the ISM to form new stars and a range of complex molecules. This continuous cycle of processing and recycling in our stellar backyard has enormous astrophysical implications, and understanding the physics and chemistry of the ISM is a key to understanding the physiochemical evolution of the galaxy and the universe.

By mass, the ISM is composed of 70% hydrogen, 28% helium and the remaining 2%

¹1 pc = 3.085×10^{16} m, 1 AU = 1.495×10^{11} m

consisting of heavy elements primarily in the form of dust. The temperature and visibility of these regions depends on the constituent material and is organized into different phases. Table 1.1 gives the physical characteristics of each of these phases. The cold dense phase, with temperatures ranging from 10 K – 300 K, is also the densest phase in the ISM. In our own Milky Way, this phase consists of:

- **Molecular Clouds (MC):** The temperatures in these clouds is in the range 10 K – 20 K, with a density of $10^2 - 10^6$ atoms/cm³. This region has the lowest volume filling factor ($f \sim 0.05$), the fractional volume of ISM that contains this material. Radio and infrared emission and absorption dust extinction are the primary tracing techniques to detect the MC regions.
- **Cold Neutral Medium (CNM):** With a density of 20–50 atoms/cm³ and temperatures in the range 50 K – 100 K, the CNM along with the MC constitute the bulk of the mass of the ISM.

The warm intercloud phase ($T \sim 10^4$ K) consists of:

- **Warm Neutral Medium (WNM):** Temperatures ranging from 6000 K – 10000 K with a low density of 0.2 – 0.5 atoms/cm³. With a filling factor of 30% of the ISM, the hydrogen constituting the WMN is in its neutral atomic state.
- **Warm Ionized Medium (WIM):** Hydrogen in the WIM is ionized, with an average temperature of 8000 K and a filling factor of 20 – 30. The primary observation techniques are H_α and pulsar dispersion, the latter manifests observationally as a broadening of an otherwise sharp pulse when observing a pulsar.
- **Ionized Hydrogen (HII):** The H II regions ($T \sim 10^4$ K) in the Milky Way are the bright visible nebulous objects like the Great Nebula in Orion are also in this phase.

The densities in the HII regions varies depending on the compactness of the region with $1 - 10^5$ atoms/cm³; so does the visibility.

The third phase is the very hot intercloud gas with temperatures on the order of a million degrees.

- **Hot Ionized Medium (HIM):** The HIM ($T \sim 10^6$ K) consists of coronal gas which has been shock heated by supernovae. The density of these regions is extremely low ($10^{-4} - 10^{-2}$ atoms/cm³) and fills 50% of the ISM.

Phase	T (K)	Density (cm ⁻³)	f(%)	M($10^9 M_{\odot}$)
Molecular Clouds (MC)	10 – 20	$10^2 - 10^6$	0.05	1.3
Cold Neutral Medium (CNM)	50 – 100	220 – 50	1.0	2.2
Warm Neutral Medium (WNM)	8000	0.2 – 0.5	30.0	2.8
Warm Ionized Medium (WIM)	8000	0.1	20 – 30	1.0
Hot Ionized Medium (HIM)	$10^6 - 10^7$	$10^{-4} - 10^{-2}$	~50	–
HII region	10^4	$1 - 10^5$	–	0.05

Table 1.1: Phases of the interstellar medium (Tielens, 2005)

Most of the information about the ISM comes from ground-based and space-based telescopes designed to detect a particular wavelength range. Radio waves, infrared and HI 21 cm absorption and emission lines, H_{α} and X-ray emission, and UV absorption lines are the observational techniques used to study different phases and components of the ISM. The light coming from the ISM spans almost the entire electromagnetic spectrum, ranging from

radio waves and infrared emissions from the molecular clouds to X-ray emission by highly charged ions in the hot gas regions.

The various components of the ISM include neutral atomic gas, ionized gas, molecular gas, coronal gas, interstellar dust, and large interstellar molecules, some of which are discussed in the following sections.

1.2 Neutral Atomic Gas : Hydrogen (H I)

In the CNM of the ISM, matter is mostly in the form of neutral hydrogen gas. In the presence of bright background stars, the neutral gas can be observed in optical and UV absorption lines of different elements. Neutral hydrogen atoms (H I) in these cold clouds have electrons in the ground state, making them difficult to observe directly. Atom-atom collisions are also rare in these conditions; however, the hyperfine splitting ($F = 0 \rightarrow 1$) of the ground state of hydrogen results in the well-known 21 cm radio waves from these H I clouds. Although the lifetime for an electron to flip its spin to emit a photon is 10^7 years, the astronomical size of these clouds results in a 21 cm line that is a good measure of the amount of H I and that is used to trace the neutral gas in the ISM (Heiles & Troland, 2004).

Atomic hydrogen is the most abundant atom in the universe (90% of atoms by number) and is the fuel for the stars and galaxies. This small and simple atom is the fundamental building block for various heavy elements formed by fusion in stars and supernovae. In gas-phase and gas-grain chemistry, the H atom is the precursor in the formation of small and large molecules in the ISM, ranging from H_2 to $CH_3OC(O)CH_3$. In chapter 3, I report on our study of the fundamental process of an H atom sticking on a dust grain, with astrophysical implications, are in their great detail.

1.3 Molecular Gas : H₂

In the molecular cloud regions of the ISM, where temperatures are around 10 K, gas-phase molecules are in their electronic and vibrational ground states. To map these regions and detect the constituent molecules, rotational transition lines (resulting from the interaction of the molecules with the electromagnetic field) are observed. However, a dominant part of the molecular gas (70% by mass), H₂, has zero electric dipole moment due to inversion symmetry, making it undetectable directly. It does have an electric quadrupole moment, but that is very weak and difficult to detect in molecular cloud regions. Molecules such as CO that coexist with H₂ are used as tracers to study the abundance and distribution of H₂ in the ISM. The abundance ratio of H₂/CO is $10^4 - 10^5$, and the 2.6 mm line for the J= 1 → 0 transition in CO is the most common tracer for H₂.

Molecular hydrogen is the simplest and most important molecule in interstellar chemistry. It is an efficient cooling agent in different environments and plays a crucial role in the macro- and micro-physical evolution of a galaxy.

- The first neutral molecule to be formed was H₂, and it played a role in the collapse of the first cosmological objects (Saslaw & Zipoy, 1967; Lepp et al., 2002).
- New stars in the molecular cloud regions of the ISM are formed by gravitational collapse of molecular gas. It is found that the mass surface density of H₂ gas correlates with the star formation efficiency in standard galaxies.
- In regions where it is too cold, and metal poor, the CO emission lines are weak or nonexistent, and the H₂ would go undetected. This could contribute significantly to the “dark” baryons in the universe, as only 8% of total expected mass is observed baryonic mass.
- During the collapse of a proto-star, planets are formed from the circumstellar disks.

These disks are composed of 99% molecular gas (mostly H_2) and 1% dust; therefore, H_2 is an important factor in the formation and dynamics of giant gas planets.

- H_2 interacting with dust surfaces creates one of the richest environments for complex molecule formation. In the dust-catalyzed astrochemistry, H and H_2 interact with dust surfaces and provide the building blocks for a complex chemical network.
- The ortho-para branching ratio of H_2 provides a means for calculating the age of molecular clouds and further influences the ortho-para ratio of other molecules.

As one can see, molecular hydrogen dominates the evolution of the galaxy at all levels, and a complete understanding of its various interactions at these levels is needed to gain a better insight into the clockwork of the universe. In chapter 4, I contribute to this complete understanding with a computational study of the sticking process of an H_2 molecule on ice.

1.4 Interstellar Dust

Although it constitutes less than 1% of the mass of ISM, dust effects the way we observe the sky using telescopes. The dominant opacity source for non-ionizing photons in the ISM is provided by dust. It absorbs high energy radiation (shorter wavelength, optical and UV) leading to heating of the dust and the subsequent emission of longer wavelength radiation (submillimeter and IR) resulting in cooling. Put together this is the extinction and reddening of the radiation, and accounts for 30% of the luminosity of the galaxy (Cunha et al., 2005). The different effects on starlight by dust provide information about the composition and properties of dust (Draine, 2003). These grains lock up a substantial portion of the heavy elements in the ISM and are composed of carbon, ices, carbides, silicon, graphite, and silicate grains. Dust provides a surface for different species to adsorb and react giving rise to a complex chemistry. The accretion and dust destruction processes also regulate the gas phase

abundance of elements.

The size of these microscopic dust grains varies from a few nanometers to 1 μm . The Mathis-Rumpl-Nordsieck (MRN) model (Mathis et al., 1977) developed for graphites and silicates gives the following dust size distribution:

$$n_i(a)da = A_i n_{\text{H}} a^{-3.5} da, \quad (1.1)$$

where a is the grain size, A_i is a constant equal to 6.9×10^{-26} and $7.8 \times 10^{-26} \text{ cm}^{2.5} (\text{H atom})^{-1}$ for graphite and silicate, respectively. This power law size distribution with an -3.5 exponent is for grain sizes in the range of $50 - 2500 \text{ \AA}$. The total number density and surface area is dominated by small grains while the total dust volume is dominated by large grains.

In the cold molecular regions of the ISM, the carbonaceous and silicate grains are covered with mantles of ice. These molecules (e.g. H_2O , CO , CO_2) either condense on or form on the grain surfaces. Absorption bands in the IR range confirm the amorphous nature of these ices. In my dissertation work, I have modeled an amorphous water ice surface to simulate a dust grain covered with layers of ice. The simulation method is discussed in Section 2.6.

1.5 Interstellar Molecules

As of March 2013, approximately 180 molecules have been detected in the ISM and circumstellar shells. Table 1.2 provides a complete list of the molecules detected so far in these regions (Müller et al., 2005). CO is the second most abundant molecule in the universe with a relative abundance of 10^{-4} with respect to H_2 , while molecules like H_2O and OH are less abundant (10^{-6}). The abundance ratio of most other species depends on the region of the ISM in which they are detected and is typically in the range $10^{-11} - 10^{-7}$ with respect to the H_2 abundance.

2 atoms	3 atoms	4 atoms	5 atoms	6 atoms	7 atoms	8 atoms	9 atoms	10 atoms	11 atoms	12 atoms	>12 atoms
H ₂	C ₃ [*]	c-C ₃ H	C ₅ [*]	C ₅ H	C ₆ H	CH ₃ C ₃ N	CH ₃ C ₄ H	CH ₃ C ₅ N	HC ₉ N	c-C ₆ H ₆ [*]	HC ₁₁ N
AlF	C ₂ H	<i>l</i> -C ₃ H	C ₄ H	<i>l</i> -H ₂ C ₄	CH ₂ CHCN	HC(O)OCH ₃	CH ₃ CH ₂ CN	(CH ₃) ₂ CO	CH ₃ C ₆ H	C ₂ H ₅ OCH ₃ [*]	C ₆₀ [*]
AlCl	C ₃ O	C ₃ N	C ₄ Si	C ₃ H ₄ [*]	CH ₃ C ₂ H	CH ₃ COOH	(CH ₃) ₂ O	(CH ₂ OH) ₂	C ₃ H ₅ OCHO	<i>m</i> -C ₃ H ₇ CN	C ₇₀
C ₂ [*]	C ₂ S	C ₃ O	<i>l</i> -C ₃ H ₂	CH ₃ CN	HC ₃ N	C ₇ H	CH ₃ CH ₂ OH	CH ₃ CH ₂ CHO			
CH	CH ₂	C ₃ S	c-C ₃ H ₂	CH ₃ NC	CH ₃ CHO	C ₆ H ₂	HC ₇ N	CH ₃ CH ₂ CHO	CH ₃ OC(O)CH ₃		
CH ⁺	HCN	C ₃ H ₂ [*]	H ₂ CCN	CH ₃ OH	CH ₃ NH ₂	C ₆ H ₂	C ₈ H				
CN	HCO	NH ₃	CH ₄	CH ₃ SH	<i>c</i> -C ₂ H ₄ O	<i>l</i> -HC ₆ H [*]	CH ₃ C(O)NH ₂				
CO	HCO ⁺	HCCN	HC ₃ N	HC ₃ NH ⁺	H ₂ CCHOH	CH ₂ CHCHO(?)	C ₈ H ⁻				
CO ⁺	HCS ⁺	HCNH ⁺	HC ₂ NC	HC ₃ CHO	C ₆ H ⁻	CH ₂ CCHCN	C ₃ H ₆				
CP	HOC ⁺	HNCO	HCOOH	NH ₂ CHO		H ₂ NCH ₂ CN	CH ₃ CH ₂ SH(?)				
SiC	H ₂ O	HNCS	H ₂ CNH	C ₅ N		CH ₃ CHNH					
HCl	H ₂ S	HOCO ⁺	H ₂ C ₂ O	<i>l</i> -HC ₄ H [*]							
KCl	HNC	H ₂ CO	H ₂ NCN	<i>l</i> -HC ₄ N							
NH	HNO	H ₂ CN	HNC ₃	<i>c</i> -H ₂ C ₃ O							
NO	MgCN	H ₂ CS	SiH ₄ [*]	H ₂ CCNH(?)							
NS	MgNC	H ₃ O ⁺	H ₂ COH ⁺	C ₅ N ⁻							
NaCl	N ₂ H ⁺	<i>c</i> -SiC ₃	C ₄ H ⁻	HNCHCN							
OH	N ₂ O	CH ₃ [*]	HC(O)CN								
PN	NaCN	C ₃ N ⁻	HNCNH								
SO	OCS	PH ₃ (?)	CH ₃ O								
SO ⁺	SO ₂	HCNO	NH ₄ ⁺								
SiN	<i>c</i> -SiC ₂	HOCN	H ₂ NCO ⁺ (?)								
SiO	CO ₂	HSCN									
SiS	NH ₂	H ₂ O ₂									
CS	H ₃ ^(*)	C ₃ H ⁺									
HF	SiCN	HMgNC									
HD	AlNC										
FeO(?)	SiNC										
O ₂	HCP										
CF ⁺	CCP										
SiH(?)	AlOH										
PO	H ₂ O ⁺										
AlO	H ₂ Cl ⁺										
OH ⁺	KCN										
CN ⁻	FeCN										
SH ⁺	HO ₂										
SH	TiO ₂										
HCl ⁺											
TiO											
ArH ⁺											

Table 1.2: List of molecules detected in the Interstellar Medium and Circumstellar Shells (Müller et al., 2005).
<http://www.astro.uni-koeln.de/cdms/molecules>

Molecules in the ISM are formed by two major classes of processes: Gas-phase chemical reactions and gas-surface chemistry. These categories are described briefly in the following sections.

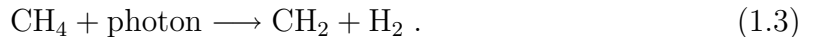
1.6 Gas-Phase Chemical Reactions

Gas-phase reactions can be broadly divided into bond-formation, bond-destruction and bond-rearrangement processes. The rate of formation or destruction for a species can be expressed in the form of a master equation as:

$$\frac{dn(A)}{dt} = -k_1n(A)n(B) + k_2n(C)n(D) + \dots \quad (1.2)$$

where k_i is rate constant, and $n(A), n(B), n(C)$ and $n(D)$ are the number densities of A, B, C and D species respectively. Specific gas-phase processes include:

- **Photodissociation:** Far ultraviolet (FUV, 6.6 eV – 13.6 eV) photons in the ISM destroy molecules with binding energies in the range 2–10 eV. An example of photodissociation reaction is



The rate constant for this process is $k_{pd} = a \exp[-bA_v]$, where a is $1 \times 10^{-9} \text{ s}^{-1}$, b is 1.7 and A_v is the visual extinction due to dust (Tielens, 2005). This is an example of a unimolecular reaction, whose rate of destruction can be expressed in a general form as:

$$\frac{dn(A)}{dt} = -kn(A) = -\frac{dn(C)}{dt} . \quad (1.4)$$

- **Neutral-neutral reactions:** These gas phase chemical reactions generally require

an exothermic transition to be efficient. An astrophysically relevant reaction network which involves the formation of water in the ISM, is



with heat of formation of 1950 K and 9610 K for OH and H₂O formation, respectively. The reaction rate is of the form $k = \alpha(T/300)^\beta \exp[-\gamma/k_B T]$ for H₂O formation, where α , β , and γ are 9.0×10^{-12} , 1.0, and 4.5×10^3 (Tielens, 2005) respectively.

- **Ion-molecule:** In the presence of cosmic rays, molecules in the ISM can be ionized, and an example of cosmic-ray driven ion-molecule reaction is



The rates for reaction 1.8, and 1.9 are $2.1 \times 10^{-9} \text{s}^{-1}$, and $8.0 \times 10^{-9} \text{s}^{-1}$ (Tielens, 2005) respectively.

- **Charge transfer:** The reaction between O and H⁺, a charge-transfer process, is of interest in the ISM:



The resulting O⁺ radical is now available to participate in a number of interstellar chemical processes. This reaction is in quasi-resonance with the reverse reaction, so

that the O^+/O abundance ratio tracks that of the H^+/H (Stancil et al., 1999).

- **Dissociative recombination:** This process involves a neutral product in an excited state that can dissociate once formed after an electron is captured by a molecular ion; for example:



Radiative-association reactions involve the collision of two species with the emission of a photon, resulting in a stable product. These along with collisional association and dissociation and associative detachment, are among the ways molecules are constantly formed and destroyed in the ISM via the gas-phase chemistry.

1.7 Grain-Surface Chemistry

The formation of a number of large, complex molecules observed in the ISM is catalyzed by dust grains. A simple and important example of how grains help in the formation of molecules is given by:



This process involves a number of steps, including the following:

- **Accretion:** The rate of accretion (k_{ac}) on a dust grain is given by (Tielens, 2005):

$$k_{ac} = n_d \sigma_d v S(T, T_d) \simeq 10^{-17} \left(\frac{T}{10 \text{ K}} \right)^{1/2} n s^{-1} \quad (1.13)$$

T and T_d are the temperatures of gas and dust respectively. Cross-sectional area of the grain is σ_d , grain number density is n_d and v is the thermal velocity of gas. The

sticking coefficient $S(T, T_d)$ depends on the temperature of gas, the type of species adsorbing and the interaction energy between the gas atom and the surface.

- **Diffusion:** Atoms or molecules that accrete on a dust grain diffuse on the surface. The interaction between the adsorbate and the surface is classified as chemisorption if a chemical bond is formed and as physisorption-typically a much weaker interaction-otherwise. Chemisorption sites on grain surfaces are quickly covered with a layer of ice in the molecular clouds, thereby making physisorption the only relevant process in molecular formation on ice mantles.
- **Reaction:** The dust grains provide a surface for the atoms and molecules to react with each other and form new molecules. Often the surface lowers the reaction activation barrier, thereby making a reaction more probable than the corresponding gas-phase process.
- **Ejection:** The newly formed molecules are then ejected back into the gas phase either by the energy released by the reaction going into kinetic energy (reaction pumping), by internal excitation of the molecule, and/or by heating of the grain. For a pure ice surface, molecules will evaporate once the temperature of the grain increases.

1.8 Sticking and H₂ formation

There are three different catalytic modes by which H atoms combine on dust surfaces to form H₂ molecules.

- **Eley-Rideal (ER) Mechanism:** In this process, the collision of an H atom from the gas-phase with an H atom already adsorbed on the surface (see Figure 1.1), results in the formation of an H₂ molecule(Eley , 1941).

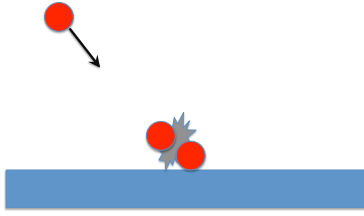


Figure 1.1: Eley-Rideal Mechanism (Eley , 1941)

- **Langmuir-Hinselwood (LH) Mechanism** : H atoms adsorbed on the surface of the dust migrate some distance, and upon encountering another H atom (see Figure 1.2), interact resulting in the formation of an H_2 molecule (Hinshelwood, 1930; Langmuir, 1922). In the dark molecular cloud conditions, the LH mechanism is the most efficient route to H_2 formation.

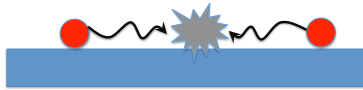


Figure 1.2: Langmuir-Hinselwood Mechanism (Hinshelwood, 1930; Langmuir, 1922)

- **Harris-Kasemo (HK) Mechanism**: An atom with hyperthermal energy bounces on the surface multiple times, losing energy each time and finally thermalizes (see Figure 1.3) with the surface temperature (Harris & Kasimo, 1981). Following which, it interacts with another H atom residing on the surface to form an H_2 molecule.

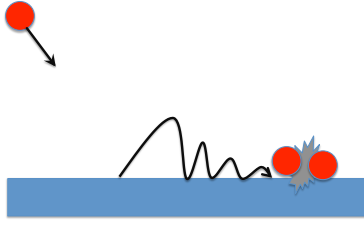


Figure 1.3: Harris-Kasemo Mechanism (Harris & Kasimo, 1981)

In all the above processes, sticking (see Figure 1.4) of an H atom on the surface is the first step in H_2 formation. Once formed, the H_2 molecule is ejected back into the gas phase where it initiates a rich gas-phase chemistry.

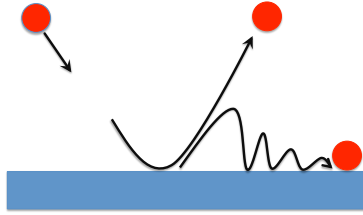


Figure 1.4: Sticking and scattering of an atom on a surface.

The rate of molecular hydrogen production R_{H_2} as expressed by Hollenbach & Salpeter (1971), is given by

$$R_{\text{H}_2} = \frac{1}{2} n_{\text{H}} v_{\text{H}} \sigma_d \gamma n_d \quad (1.14)$$

where n_{H} (cm^{-3}) is the number density of H atoms, v_{H} (cm s^{-1}) is the speed of H atoms in gas phase, σ_d (cm^2) is the average cross-sectional area of the grain, and n_d (cm^{-3}) is the number density of dust grains. The symbol γ represents the fraction of H atoms striking the grain that eventually form H_2 and $\gamma = S\eta$, where S is the sticking coefficient and η is the

probability that an H atom on the surface will react with another adsorbate to form a new molecule. The sticking coefficient is deduced either theoretically or experimentally, and it determines the molecular-hydrogen formation rate.

Equation 1.14 does not take the dust grain properties into account and Le Bourlot et al. (1995b) have shown that the rate of H₂ formation can be expressed in terms of the dust size and mass distribution.

$$R(H_2) = \frac{1}{2} S \frac{3 \times 1.4 m_H G}{4 \rho_{gr} \sqrt{a_{min} a_{max}}} \times \sqrt{\frac{8k}{\pi m_H}} \times \sqrt{T} n(H) n_H \quad (1.15)$$

where S is the sticking coefficient, ρ_{gr} is density of grain, a_{min} and a_{max} are minimum and maximum radii of the grain, respectively, and G is the dust-to-gas mass ratio.

The goal of my PhD work has been to predict the sticking coefficients for different atoms and molecules by studying their interaction with dust grain surfaces. In Chapter 2, I briefly discuss the computational tool used to study the sticking process and the "nuts and bolts" of the Molecular Dynamics simulation technique.

In Chapter 3, I report in detail the study of the sticking process of an H atom on ice surfaces at different temperatures. We have computed the sticking probabilities for a range of incident gas energies and deduced the sticking coefficients.

In Chapter 4, the H₂ sticking probability is estimated on a 10 K ice surface and the thermally averaged sticking coefficients determined. My conclusions and future work are briefly discussed in Chapter 5.

Chapter 2

Molecular Dynamics Simulations

2.1 Introduction

Computer simulations act as a bridge between theory and experiment, microscopic and macroscopic properties. They are used extensively to test and construct approximate theories, compare with theoretical predictions and real experiments, and design better models and experiments. Classical molecular dynamics (MD)(Allen & Tildesley, 1987; Rappaport, 2004) and Monte-Carlo (MC) simulations (Landau & Binder, 2009) are two common methods used to model and study interactions between electrons, atoms and molecules to predict bulk properties. A combination of MC and MD is used to model systems where both equilibrium and dynamic properties are of interest. Simulations provide a tool to conduct new physics research in areas where conventional theory and experiments cannot make much progress. For example, in extreme conditions of temperature, pressure, and density, experiments are quite difficult and therefore rare. In these situations, computer simulations are virtually the only way we can peek into the behavior and properties of a system.

Simulations attempt to mimic the behavior of macroscopic systems by carefully modeling the interactions at a microscopic level and thereby investigate the resulting phenomena.

Classical MD is in many ways similar to designing a very detailed experiment, where we specify exactly the number of atoms (N) in the experiment and the various interactions the constituent particles partake in. In simple terms, MD is a numerical step-by-step solution of Newton's classical equations of motion for a large system of interacting particles:

$$\begin{aligned} m_i \ddot{\vec{r}}_i &= \vec{f}_i, \\ \vec{f}_i &= -\vec{\nabla} \mathcal{U}, \end{aligned} \tag{2.1}$$

where \vec{r}_i is the position of and \vec{f}_i the force acting on the i -th particle, with mass m_i and acceleration $\ddot{\vec{r}}_i$. In order to solve equation 2.1, we need to model the potential energy \mathcal{U} of the interacting particles in the system. *Ab initio* calculations provide highly accurate potential energy hyper-surfaces for relatively small atom-atom systems or molecular clusters. However, to study the bulk properties of a large system (10^3 atoms or more), simpler phenomenological potential energy functions, for example a Lennard-Jones (1936) potential form, are needed to make the simulations computationally tractable.

2.2 Interaction Potentials

For simplicity, we will consider atomic systems with non-bonded interactions. A more rigorous treatment of bonded and non-spherical systems can be found in Allen & Tildesley (1987). Non-bonded interactions in a system of atoms can be expressed in terms of 1-body, 2-body, 3-body and higher order interaction potentials in the form:

$$U_{non-bonded} = \sum_i u(\vec{r}_i) + \sum_i \sum_{j>i} u(\vec{r}_i, \vec{r}_j) + \sum_i \sum_{j>i} \sum_{k>j>i} u(\vec{r}_i, \vec{r}_j, \vec{r}_k) + \dots \tag{2.2}$$

where $u(\vec{r}_i)$ is an externally applied potential field, $u(\vec{r}_i, \vec{r}_j)$ is a pair potential, $u(\vec{r}_i, \vec{r}_j, \vec{r}_k)$ is a 3-body interaction and so on so forth. The notation $\sum_i \sum_{j>i}$ indicates the summation is over all distinct pairs i and j without counting any pair twice and $\sum_i \sum_{j>i} \sum_{k>j>i}$ notation for the triplets without counting any triplet 3 times. The physics of a simple system can be studied using the first two terms, and the 3-body and higher order terms are often neglected. However, higher order contributions like 3-body effects can be partially included by defining an 'effective' potential by rewriting Equation 2.2 as:

$$U_{non-bonded} \approx \sum_i u(\vec{r}_i) + \sum_i \sum_{j>i} u^{\text{eff}}(\vec{r}_i, \vec{r}_j), \quad (2.3)$$

where u^{eff} is a pair potential designed to partially incorporate key many-body effects.

To simulate atomic systems, continuous and differentiable interaction potentials are used. A simple and commonly used pair potential is the Lennard-Jones (LJ) potential which is in the form:

$$v^{\text{LJ}}(r) = 4\epsilon \left[\left(\frac{\sigma}{r} \right)^{12} - \left(\frac{\sigma}{r} \right)^6 \right], \quad (2.4)$$

where r is the interatomic distance, ϵ is the depth of the potential well and σ is the finite distance at which the inter-particle potential equals zero. The r^{-12} term is the repulsive part, taking into account Pauli repulsion at short distances due to overlapping electron orbitals. The van der Waals induced dipole-dipole interaction is modeled by the attractive r^{-6} term.

For small systems, one can sum over all the constituent pairs to calculate the total potential energy. With the increase in system size, the number of computations (N^2) increases with not so significant gain in accuracy. One way to resolve this inefficiency is to use a cut-off distance to calculate the potential energy and ignore the interaction effects from any pair separated by more than the cut-off radius. This reduces the number of pair interactions that need be computed at each step and speeds up the program. However, the truncation of

the interaction potential introduces a discontinuity in the potential function, and whenever a pair of molecules cross this boundary, the total energy of the system is not conserved. This can be avoided by shifting the potential by $v_c = v(r_c)$, where $v(r_c)$ is the potential at the cut-off distance. The shifted LJ potential is:

$$v^S(r_{ij}) = \begin{cases} v(r_{ij}) - v_c & r_{ij} \leq r_c \\ 0 & r_{ij} > r_c \end{cases} . \quad (2.5)$$

The force calculated using the shifted LJ potential is still discontinuous at $v_c = v(r_c)$ and can cause instability in the numerical solutions of the equations of motion. A 'shifted force pair-potential' can avoid this difficulty by adding a linear term to the potential. The derivative of the following expression is zero at r_c

$$v^{\text{SF}}(r_{ij}) = \begin{cases} v(r_{ij}) - v_c - \left(\frac{dv(r_{ij})}{dr_{ij}} \right)_{r_{ij}=r_c} (r_{ij} - r_c) & r_{ij} \leq r_c \\ 0 & r_{ij} > r_c \end{cases} . \quad (2.6)$$

Another trick to reduce the number of computations is to use neighbor lists. In a MD program, at each step, an atom i and a loop over all atoms j is considered to find the separation distance r_{ij} . When the separation distance is greater than the potential cut-off, the program skips avoiding expensive calculations. To speed up further, Verlet (1967) suggested keeping a list of the neighbors for each particle that is updated at regular intervals. In a three-dimensional cell, this method reduces the number of calculations from N^2 (by summing over all i and j) to $27NN_c$, where $N_c = N/M$ and M is the cut-off radius cell.

In systems with electrostatic forces, electric potential energy is calculated according to:

$$v^{\text{Coulomb}}(r_{ij}) = \frac{kq_i q_j}{r} , \quad (2.7)$$

where q_i and q_j are the charges on particle i and j respectively. For electrostatic interactions,

for which the Coulomb potential decays slowly, using a cutoff radius introduces non-physical behavior. For potentials like these, the long range forces are calculated using Ewald (1921) summation method, a technique developed to find the sum between an ion and all its periodic images. This is an efficient yet accurate way of calculating the long range forces by using reciprocal-space vectors. Using this method, total potential energy contains a real-space sum and a reciprocal-space sum, minus an error function.

2.3 MD Algorithm

For a simple atomic system with N atoms, the positions and momenta are \vec{r}_N and \vec{p}_N respectively. The kinetic energy of the system is $\mathcal{K} = \sum_i^N p_i^2/2m_i$, where m_i is the mass of the i th atom and \vec{p}_i is its momentum. The Hamiltonian of the system is $\mathcal{H} = \mathcal{K} + \mathcal{U}$, and the equations of motion are:

$$\begin{aligned}\dot{\vec{r}}_i &= \frac{\vec{p}_i}{m_i}, \\ \dot{\vec{p}}_i &= \vec{f}_i.\end{aligned}\tag{2.8}$$

The above coupled differential equations are then solved using a step-by-step numerical integration method. Pseudo code for a simple MD code is given in Algorithm 2.1 and lists the various steps involved. The observables in a MD simulation are all expressed in terms of position, velocities or momenta, e.g., to calculate temperature (T), the equipartition energy over all degrees of freedom is used. The average kinetic energy per degree of freedom is

$$\left\langle \frac{1}{2}mv_i^2 \right\rangle = \frac{1}{2}k_B T.\tag{2.9}$$

To initialize a system with a given temperature, we use Equation 2.9 to assign the magnitude of velocities of the atoms. The instantaneous temperature of the system at a given time t is then given as:

$$T(t) = \frac{1}{k_B N_f} \sum_i^N m_i v_i^2(t) , \quad (2.10)$$

where N_f is number of degrees of freedom. The temperature of the system is then computed by averaging over a sufficiently long time interval.

Algorithm 2.1 Simple MD pseudo code

Begin Program

Initialize ▷ Initialize positions and velocities

$t \leftarrow 0$

while $t \leq t_{max}$ **do** ▷ Repeat until the maximum simulation time

Calculate Force ▷ Derivative of the interaction potential

Integrate (update r_i, v_i, a_i) ▷ Integrate equations of motion

$t \leftarrow t + \Delta t$ ▷ Increment the time step

Sample Observables ▷ Calculate energy, temperature, pressure

end while

Calculate Averages

End Program

2.4 Time Integration Algorithms

With the positions and velocities of the atoms initialized, the potential energy is calculated from the selected model interaction, and the atomic forces are determined from its gradient. The engine of a MD simulation lies in the numerical integration method employed to update the position, velocity, and acceleration of each individual atom with the evolution of time. An ideal integration scheme must result in a constant energy for the system over long times and accurate calculation of the dynamical quantities of interest. The velocity Verlet algorithm has been optimized to achieve these goals in solving the classical equations of motion.

To arrive at the Verlet algorithm, we start with a simple Taylor expansion for the position $\vec{r}_i(t)$ in two directions. In the forward direction of time t with an increment Δt , we have:

$$\vec{r}_i(t + \Delta t) = \vec{r}_i(t) + \vec{v}_i(t)\Delta t + \frac{1}{2}\vec{a}_i(t)\Delta t^2 + \frac{1}{6}\vec{b}_i(t)\Delta t^3 + \mathcal{O}(\Delta t^4), \quad (2.11)$$

and in the backward direction of time with a decrement of Δt gives:

$$\vec{r}_i(t - \Delta t) = \vec{r}_i(t) - \vec{v}_i(t)\Delta t + \frac{1}{2}\vec{a}_i(t)\Delta t^2 - \frac{1}{6}\vec{b}_i(t)\Delta t^3 + \mathcal{O}(\Delta t^4). \quad (2.12)$$

Adding and rearranging Equations 2.11 and 2.12 gives the following:

$$\vec{r}_i(t + \Delta t) = 2\vec{r}_i(t) - \vec{r}_i(t - \Delta t) + \vec{a}_i(t)\Delta t^2 + \mathcal{O}(\Delta t^4). \quad (2.13)$$

This is the Verlet algorithm in its basic form. The MD method relies on the velocity calculations to compute temperature and kinetic energy. The velocity can be estimated using the mean value theorem and the position terms as:

$$\vec{v}_i(t) = \frac{\vec{r}_i(t + \Delta t) - \vec{r}_i(t - \Delta t)}{2\Delta t} + \mathcal{O}(\Delta t^2), \quad (2.14)$$

where the error associated with the velocities is $\mathcal{O}(\Delta t^2)$ rather than $\mathcal{O}(\Delta t^4)$. The leap-frog

algorithm handles velocities better. In this scheme, the positions are advanced from $\vec{r}_i(t)$ to $\vec{r}_i(t + \Delta t)$ and the velocities from $\vec{v}_i(t + \frac{1}{2}\Delta t)$ to $\vec{v}_i(t + \frac{3}{2}\Delta t)$, hence the term leap-frog. The following equations for position and velocity are used in the leap-frog method:

$$\begin{aligned}\vec{r}_i(t + \Delta t) &= \vec{r}_i(t) + \vec{v}_i(t + \frac{1}{2}\Delta t)\Delta t, \\ \vec{v}_i(t + \frac{3}{2}\Delta t) &= \vec{v}_i(t + \frac{1}{2}\Delta t) + \frac{1}{m}\vec{f}_i(\vec{r}_i(t + \Delta t))\Delta t.\end{aligned}\tag{2.15}$$

A modified form of the Verlet algorithm, known as the velocity Verlet algorithm is more often used in MD simulations. Equation 2.16 gives a step-by-step process to update positions, velocities and accelerations as:

$$\begin{aligned}\vec{r}_i(t + \Delta t) &= \vec{r}_i(t) + \vec{v}_i(t)\Delta t + \frac{1}{2}\vec{a}_i(t)\Delta t^2, \\ \vec{v}_i(t + \frac{1}{2}\Delta t) &= \vec{v}_i(t) + \frac{1}{2}\vec{a}_i(t)\Delta t, \\ \vec{a}_i(t + \Delta t) &= -\frac{1}{m}\vec{f}_i(\vec{r}_i(t + \Delta t)), \\ \vec{v}_i(t + \Delta t) &= \vec{v}_i(t + \frac{1}{2}\Delta t) + \frac{1}{2}\vec{a}_i(t + \Delta t)\Delta t.\end{aligned}\tag{2.16}$$

The time step Δt is used to propagate the equations of motion in steps which ignore the kinetic and potential part of the hamiltonian. Only when $\Delta t \rightarrow 0$, we can truly conserve energy. However, velocity-Verlet-like algorithms provide a very a good approximation that come very close to achieving constant-energy states. This enables us so to carry out a constant energy (E), fixed volume (V) and fixed number of particles (N), or a NVE , simulation. The time step $\Delta t = t/n_{steps}$, where n_{steps} is the number of steps and t the total time of simulation. An appropriate time step Δt is chosen by varying Δt so that the total energy of the system is conserved to a desired level of accuracy ($\sim 10^{-5}$). For typical atomic and molecular systems, a time step of $\Delta t \sim 10^{-15}$ s or less is used. In my study, I used a time step of 0.5 fs and the simulation time varied from 5–150 ps.

2.5 Constant-temperature MD

To simulate real experiments, it is useful to run a MD simulation at a constant temperature or pressure. The MD method can be adapted to sample from a constant-temperature ensemble to simulate a canonical ensemble with fixed number of particles, fixed total volume, and a constant temperature (T), known as NVT simulation. A simple and crude method widely used to bring a system to a desired temperature (T), from the current temperature (\mathbb{T}), is by using a scaling factor of $(T/\mathbb{T})^{1/2}$ at every t_n steps of the simulation. This is known as velocity rescaling and the kinetic temperature of a system is readjusted by using a simple velocity rescaling of all the particles in the system.

A constant temperature dynamics can be generated using the equations of motion instead of directly scaling the velocities. A number of methods exist to simulate a MD system at constant-temperature using a thermostat (Allen & Tildesley, 1987), and I describe one method used in this work.

2.5.1 Nosé-Hoover method

An extended Lagrangian method is one where a degree of freedom is included to represent the reservoir (a heat source or sink). This extended system is used to carry out the MD simulation with the modified equations of motion:

$$\begin{aligned}\dot{\vec{r}}_i &= \vec{p}_i/m_i, \\ \dot{\vec{p}}_i &= \vec{f}_i - \zeta \vec{p}_i, \\ \dot{\zeta} &= \frac{N_f}{Q} (k_B \mathbb{T} - k_B T),\end{aligned}\tag{2.17}$$

where the extra degree of freedom ζ is a frictional coefficient and Q is the associated inertia parameter. The thermostat relaxation time τ_T depends on the inertia parameter (Q), and by adjusting τ_T , the flow of energy between the system and reservoir can be controlled.

The simulation reaches an equilibrium state with constant temperature by adjusting the relaxation time τ_T . A high value of τ_T will result in very slow flow of energy between the system and the reservoir, whereas a too low value of τ_T will lead to an oscillating temperature. This is the Nosé-Hoover thermostat method which uses the equations of motion to generate a constant-temperature dynamics.

2.6 Amorphous Solid Water Simulation

Dust in the ISM may consist of silicate grains, carbon grains, or often a grain covered with multiple layers of amorphous water ice (Hagen et al., 1981). The average grain size of a dust particle is around $0.1 \mu\text{m}$ (Weingartner & Draine, 2001), although there is a large variation in the size and density of the dust particles present in the ISM. Surface interactions between an adsorbing hydrogen atom or molecule and amorphous water ice result in physisorption (Zangwill, 1988), as chemical reaction between the grain and the impinging atom is not present. Thus, to understand the atomic sticking process on ice-clad interstellar dust, we need to study the various physical processes of an adsorbing atomic species on the surface of amorphous water ice.

To simulate the grain surface, we have constructed an amorphous water ice slab, which is a good model for studying surface interactions. The interaction potential used for a pair of water molecules is the TIP4P (Transferable Intermolecular Potential) model (Jorgenson, 1982), which was also adopted in most earlier simulations of water ice. This four-site model consists of a Lennard-Jones (LJ) site at the oxygen atom and three charge sites: a positive charge on each of the hydrogen atoms and a negative charge on the H-O-H molecular angle bisector, 0.15 \AA from the oxygen atom (see Figure 2.1). The dummy atom with a positive charge improves the electrostatic distribution around the water molecular compared to the

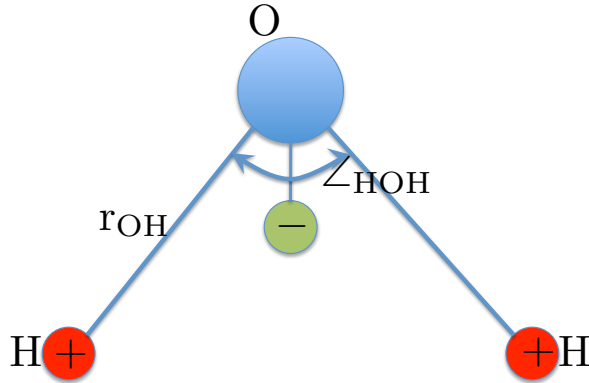


Figure 2.1: Water molecule in a TIP4P model (Jorgenson, 1982). The positive charges are on the H atoms and negative charge is displaced by 0.15 \AA from the O atom. The O–H bond distance is 0.9572 \AA and the H–O–H angle is 104.52°

three-site models (e.g., TIP3P, SPC). The potential is given by

$$V_{\text{H}_2\text{O}-\text{H}_2\text{O}} = \sum_{i,j} \frac{q_i q_j e^2}{r_{ij}} + 4\epsilon \left[\left(\frac{\sigma}{r} \right)^{12} - \left(\frac{\sigma}{r} \right)^6 \right], \quad (2.18)$$

where r is the distance between the two oxygen atoms, r_{ij} is the distance between positions i and j ; where i and j each run over the three charge positions on each of the two interacting H_2O molecules, respectively. The Lennard-Jones constants for the O–O interaction are $\sigma = 3.1536 \text{ \AA}$ and $\epsilon = 0.1550 \text{ K}$. The fixed H–O–H angle is 104.52° , and $r_{\text{O-H}} = 0.9572 \text{ \AA}$ is the fixed length of each O–H bond. The charges associated with the O and H atoms are -1.040 and 0.520 , respectively. To generate a slab of amorphous ice, we use 1000 water molecules in a simulation box, with periodic boundary conditions in the x , y , and z directions to emulate an infinite surface. The dimensions of the simulation box are $40 \text{ \AA} \times 40 \text{ \AA} \times 40 \text{ \AA}$, and the coordinates of the water molecules are randomly chosen within a region of dimension 40 \AA

$\times 40 \text{ \AA} \times 20 \text{ \AA}$ (see Figure 2.2). The restriction on the initial z -coordinate is designed to break the symmetry in the z direction. This asymmetry helps in the formation of the slab structure instead of a cube structure, leaving an empty space of 10 \AA on each side of the slab in the z direction.

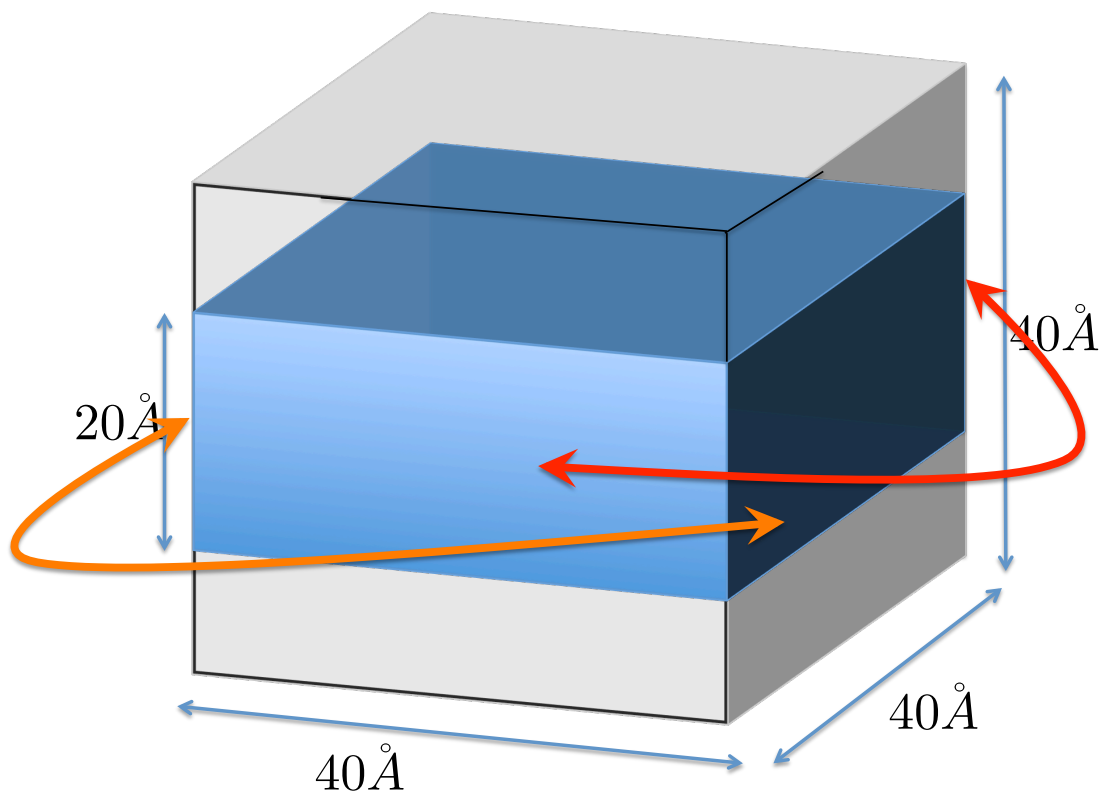


Figure 2.2: Cubic simulation box of dimensions $40 \text{ \AA} \times 40 \text{ \AA} \times 40 \text{ \AA}$ with the slab dimensions $40 \text{ \AA} \times 40 \text{ \AA} \times 20 \text{ \AA}$. Periodic boundary conditions are applied only in x and y directions and removed in the z direction once the slab has been simulated.

Once the random initial coordinates and velocities of the water molecules are set, the equations of motion are solved using the leap-frog algorithm described in Section 2.4. The

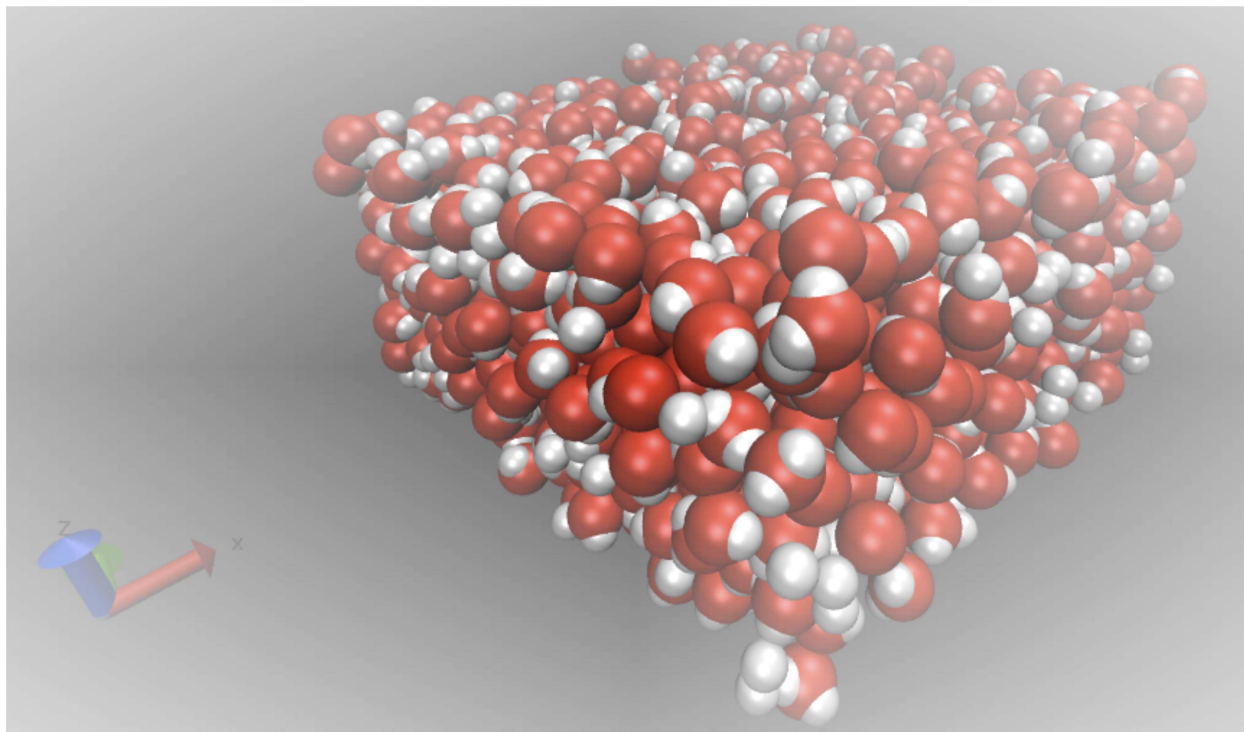


Figure 2.3: A view of the simulated amorphous water ice slab at 10 K. Red and grey balls represent oxygen and hydrogen atoms, respectively.

water molecules are treated as rigid, and hence the constraint forces are satisfied using the SHAKE algorithm (Ryckaert et al., 1977), a two-step method based on the Verlet integration scheme. In the first step, the equations of motion of all the atoms in the system are treated assuming an absence of rigid bond forces. In the following step, the constraint force is retroactively computed using the deviation in the length of the rigid bond (in our case, r_{OH}). Using this constraint force, the bond length is fixed iteratively to a tolerance level ($10^{-4} - 10^{-6} \text{ \AA}$).

A cut-off distance of 10 \AA was used for real space Coulomb interaction calculations, and Ewald summation was performed to calculate the long-range electrostatics. The system was allowed to evolve for 150 ps at a constant temperature of 300 K using a simple velocity

rescaling, and then sequentially cooled to 200 K, to 100 K, and finally to 10 K. At each of these steps the system was run for 150 ps, and the system was allowed to run in NVE for 50 ps before carrying out the next temperature scaling. The sequential procedure described above was also carried out to produce an ice slab at an end temperature of 70 K. This procedure of simulating ice was chosen to arrive at an amorphous surface and avoid unphysical behavior of the system due to numerical instabilities. Once the ice slabs were generated, the periodic boundary condition on the z direction of the slab was removed for the H-ice and H₂-ice simulations, so as to avoid the possibility of a scattered hydrogen atom or molecule re-entering the simulation box multiple times. For a fixed slab temperature, the same ice slab with identical initial H₂O positions and velocities was used for all the different incident H-atom trajectory calculations. Figure 2.3, shows an amorphous water ice slab at 10 K consisting of 1000 water molecules simulated using the above procedure.

To study the sticking of molecular hydrogen on amorphous ice (Chapter 4), I used an open source MD simulation package, the Large-scale Atomic/Molecular Massively Parallel Simulator (LAMMPS), developed by Plimpton (1995).

Chapter 3

Sticking of Atomic Hydrogen

1

3.1 Introduction

Gas-phase and gas-grain chemical networks have been invoked to explain the formation mechanism of over 140 molecules (e.g., Garrod et al., 2008; Millar et al., 1991; Herbst et al., 1997) that have been observed in molecular clouds of the interstellar medium (ISM). Molecular hydrogen is one of the most important molecules in this network and is a precursor to a number of molecules found in the ISM. The observable abundance of molecular hydrogen in the ISM cannot be entirely explained from gas-phase reactions (Glover, 2003), and hence the study of H₂ formation via gas-grain processes has key astrophysical applications. There is continued interest (Le Bourlot et al., 2012; Iqbal et al., 2012) to study and understand the interaction of hydrogen atoms on grain surfaces to explain H₂ formation using both theoretical and experimental methods. One of the fundamental steps in the H₂ formation process is the sticking of atomic hydrogen onto the grains (Cazaux et al., 2011). Dense molecular clouds in cold regions of the ISM have dust grains covered with layers of ice

¹This chapter is based on the publication Veeraghattam et al. (2014)

(Hollenbach et al., 2009) of thickness about $0.1 \mu\text{m}$ which act as a surface for the H_2 formation process.

Hollenbach & Salpeter (1970) studied the surface adsorption of gas atoms on a crystal surface and found quantum mechanical solutions. The sticking coefficient $S(T)$ for incident gas atoms is the average of adsorption probability over the thermal energy distribution of incident gas atoms,

$$S(T) = \int_0^\infty \epsilon e^{-\gamma\epsilon} P(\epsilon) d\epsilon \Big/ \int_0^\infty \epsilon e^{-\gamma\epsilon} d\epsilon \quad (3.1)$$

where $P(\epsilon)$ is the adsorption or sticking probability, T the gas temperature, and $\gamma \equiv E_c/kT$. The variable ϵ is defined as $\epsilon = E_i/E_c$, where E_i is the incident particle energy, $E_c = \Omega(D\Delta E_s)^{1/2}$, and ΔE_s is the energy transferred in a single collision,

$$\Delta E_s = M_g/M_s(E_i + D)2[\omega_0^2/(\omega^2 - \omega_0^2)]^2 \quad (3.2)$$

The parameter D is the well depth of the adsorption potential, and Ω^2 is close to unity for Lambert's law and equals 2 for isotropic scattering. The mass of gas atom or molecule is M_g , mass of the surface atom or molecule is M_s and ω the Debye frequency of the solid. Equation 3.1 can be approximated as

$$S(T) \approx (\gamma^2 + 0.8\gamma^3)/(1 + 2.4\gamma + \gamma^2 + 0.8\gamma^3), \quad (3.3)$$

where γ is dependent on the incident atom or molecule species and the type of grain surface. This approximation is often used in astrophysical models, although experiments suggest (Manico et al., 2001) that it underestimates the sticking of atomic hydrogen on interstellar ice grains. Following the seminal work of Hollenbach & Salpeter (1970), there were more specific studies involving amorphous water ice and H atoms using both computational and experimental methods to simulate the conditions in the ISM.

Buch & Zhang (1991) studied the sticking of H and D atoms on a cluster of amorphous water ice consisting of 115 water molecules using the classical molecular dynamics (MD) method. A larger system with an amorphous water ice slab of 1000 water molecules was studied in MD simulations by Masuda et al. (1998) to find the sticking and mobility of H atoms on ice. Al-Halabi et al. (2002) and Al-Halabi & van Dishoeck (2007) performed MD simulations to study the sticking of atomic hydrogen on crystalline and amorphous surfaces, respectively. Experiments carried out by Manico et al. (2001), Hornekær et al. (2003), and Watanabe et al. (2010) observed H₂ formation on ice surfaces and measured the recombination energy. The sticking coefficient of atomic hydrogen on interstellar ices was then estimated indirectly using the recombination energy from the H₂ formation process.

The sticking of atomic hydrogen on interstellar dust grains leads to the formation of molecular hydrogen via three known mechanisms. In the Eley-Rideal mechanism (Eley , 1941) an impinging hydrogen atom directly hits a hydrogen atom already on the surface and forms H₂. The Langmuir-Hinshelwood (LH) mechanism (Hinshelwood, 1930; Langmuir, 1922) involves two hydrogen atoms already on the dust surface diffusing some distance on it before reacting to form H₂. In the hot-atom mechanism (Harris & Kasimo, 1981) an impinging hydrogen atom travels at hyperthermal energy before hitting an already adsorbed atom to form H₂ and then is trapped on the dust surface. In all of these mechanisms of H₂ formation, one or more hydrogen atoms reside on the dust surface for some time before the hydrogen atoms recombine to form H₂. Thus studying the sticking probability of atomic hydrogen is an important part of understanding the H₂ formation on dust and ice grains in the ISM.

Most astrophysical models assume the sticking coefficient for various atoms and molecules to be either 1 or 0.5 (Le Bourlot, 2000). In some analytical models (Le Bourlot et al., 2012), the sticking coefficient decreases as $1/\sqrt{T}$ for gas temperatures above 10 K and a sticking coefficient of 1 at 10 K is used. While this approximation works well for low gas and grain

temperatures, we will show that it underestimates sticking at higher gas temperatures and it neglects the dependence on grain temperature. In the present study, we carry out extensive MD simulations to predict the sticking probability of atomic hydrogen on an amorphous water ice slab, for a wide range of H atom incident kinetic energies, 10 K - 600 K, and two different grain temperatures, 10 K and 70 K. The Cold Neutral Medium (CNM) and the Molecular Clouds (MC) have a temperature range from 10-100 K, which is where most of the gas-grain chemistry occurs. Studies by Cuppen et al. (2010) show significant sticking for cold dust and gas while Cazaux et al. (2011) show significant sticking for intermediate gas and dust temperatures ($100 \text{ K} < T_{gas} < 1000 \text{ K}$). Also, previous studies (Al-Halabi et al., 2002; Al-Halabi & van Dishoeck, 2007) have data points included a 600 K incident energy and we compare our data with these results.

We also address the wide range of values in the calculated and measured sticking probability in the various computational and experimental studies mentioned above. Section 3.2 explains the methodology we have used for studying this system, while the results of our simulations are presented in section 3.3. Discussion and comparison of our results with previous studies is given in section 3.4.

3.2 Methodology

We study the dynamical interactions of a hydrogen atom with an amorphous ice substrate using classical MD simulations (Allen & Tildesley, 1987, and references therein). Although this method treats the motion of atoms and molecules classically, it nevertheless has provided excellent results and predictions in the field of physical chemistry and continues to be an important computational tool to study many complex systems, including surface processes. In the context of gas-grain interactions in astrophysics, MD has been used extensively to simulate different ice and grain surfaces and then study the interactions of these surfaces

with atoms and molecules (Kroes & Clary, 1992; Andersson et al., 2006). These classical trajectory calculations have provided insight into the various grain-mediated mechanisms that are involved in the physics of the ISM.

The MD technique involves numerically integrating Newton’s equations of motion for a system consisting of many interacting particles. The positions, velocities, and forces on each atom in the system are dynamically calculated at each step of the simulation as a function of time. For a solid-state or molecular system, this involves computing the forces on each atom, which in turn are calculated from the potential energy. For non-spherical systems including rigid molecules, which have rotational degrees of freedom, the rotational equations of motion are also solved. Pairwise potentials governing the particle interactions are generally deduced from high-level quantum chemical calculations for a single pair of particles. From these potentials, an interaction force field is obtained, which is then used in MD simulations to solve the equations of motion. The set of coupled differential equations is solved by numerical integration methods, such as the velocity Verlet algorithm. Bonded molecular systems introduce constraints on the coordinates resulting in constraint forces. These constraints are satisfied exactly at the end of each time step in the simulations using schemes like SHAKE (Allen & Tildesley, 1987). While MD simulations are most naturally carried out for a microcanonical ensemble (NVE), simulations for a canonical ensemble (NVT) are made possible using numerical thermostat techniques. The algorithm and methods used are explained in more detail in Chapter 2.

For the current study, we used two different interaction potentials, one to model the water-water interaction to simulate the amorphous water ice substrate and another to model the hydrogen-water interaction to study the sticking dynamics of a hydrogen atom on the ice surface. The initial positions and velocities of the water molecules were randomly assigned, and the Leap-Frog algorithm was used to calculate these variables as the simulation evolved over time. The initial speed of the H atom is set by the incident kinetic energy, and its

incident direction of motion and initial xy coordinates are chosen at random. An NVT simulation is used to simulate the water ice slab at the desired temperature, and then NVE simulations were performed after the H atom was introduced, to study the change in energy of the H atom and the surface with time.

3.2.1 Hydrogen Interaction with Water Surface

To simulate the interaction of atomic hydrogen with the ice surface, we use the interaction potential developed by Zhang et al. (1991). Using open-shell Hartree Fock (UHF) and fourth order Møller-Plesset perturbation (MP4) theory, Zhang et al. computed the *ab initio* potential energy surface of the rigid water molecule-atomic hydrogen system. The *ab initio* data were fitted to a Lennard-Jones form given by

$$V_{\text{H-H}_2\text{O}} = \sum_{l,m} 4\epsilon_{l,m} \left[\left(\frac{\sigma_{l,m}}{r} \right)^{12} - \left(\frac{\sigma_{l,m}}{r} \right)^6 \right] Y_{l,m}(\theta, \phi) \quad (3.4)$$

with the fit parameters given in Table 1. The distance r in the LJ potential is the distance between the incident hydrogen atom and the oxygen atom. The coordinates θ and ϕ are the spherical angles of the incident hydrogen atom with respect to the water molecule, where the origin is at the oxygen atom and the polar axis coincides with the molecular symmetry axis. In the water molecule, the distance of the two H atoms is 0.9572 \AA from the oxygen center with polar angles of $\theta = 127.74^\circ$ and $\phi = \pm 90^\circ$.

At the beginning of each trajectory, a hydrogen atom is placed at a height of 9 \AA above the surface of the amorphous ice slab, where the surface normal is taken to be the z axis. The x and y coordinates of the H atom and its initial direction of motion are randomly chosen, and the magnitude of the initial velocity is set to correspond to the incident kinetic energy. Using the above H-H₂O potential, the forces on the H atom due to the water molecules in the ice surface are calculated. These forces are then used to update the positions and

l, m	$\epsilon_{l, m} [\text{K}]$	$\sigma_{l, m} [\text{\AA}]$
0, 0	222.1	3.33
1, 0	-19.6	3.00
2, 0	17.7	2.98
2, 2	73.3	2.92

Table 3.1: Parameters for the H-H₂O interaction potential (Zhang et al., 1991).

velocities of the H atom and the water molecules using the Verlet algorithm. This process was repeated for hundreds of trajectories with different initial coordinates and initial H atom velocity directions chosen randomly. The kinetic energy of the H-atom was varied from 10 K to 600 K while keeping the substrate temperature fixed at 10 K. To study the effects of the grain temperature on the sticking, the whole process was repeated for a substrate temperature of 70 K.

3.2.2 Sticking Probability

The sticking probability $P(E)$ is defined in this work as the ratio of the number of trajectories in which the hydrogen atom sticks on the surface to the total number of trajectories. A sticking event occurs when the H atom stops bouncing on the surface and remains stuck for the rest of the simulation. We have varied the length of the simulation time over the range 5 ps to 20 ps, and observe that the sticking remains independent of simulation time. To study the effect of the integration time step on the sticking process, we varied this parameter from

0.01 fs to 1 fs. For time steps smaller than 0.5 fs, the trajectories are nearly identical, the sticking process is independent of time step, and energy of the system is well conserved. Hence we used a time step of 0.5 fs for our simulations.

To find the sticking probability, we ran 200-400 trajectories (depending on the substrate temperature) for each kinetic energy E of the incident H atom on amorphous water ice slabs at 10 K and 70 K. The sticking or scattering status for these trajectories were determined. Each trajectory resulting in a sticking or a scattering process is an independent event. To estimate errors, a random sample of 50 trajectories were selected from the entire pool and average sticking probability was computed. This sampling process was repeated multiple times to get a mean and standard deviation for the sticking coefficient for each incident kinetic energy.

3.3 Results

The dense cold molecular clouds and the cold neutral medium of the ISM have a temperature range from 10 K to 100 K, where one can find dust covered with layers of amorphous ice. Studies by Cuppen et al. (2010) and Cazaux et al. (2011) for sticking on graphite surfaces show significant sticking for intermediate gas temperatures as well. For the current study, we chose incident energies of the H atom in the range 10 K to 600 K. The higher end of the incident energy was chosen to study the effect of large incident kinetic energy on sticking and also to compare with previous computational studies. The sticking probabilities obtained from the current simulations are shown in Figure 3.1 for the 10 K ice slab and Figure 3.2 for the 70 K ice slab. These plots also show results from previous computational studies.

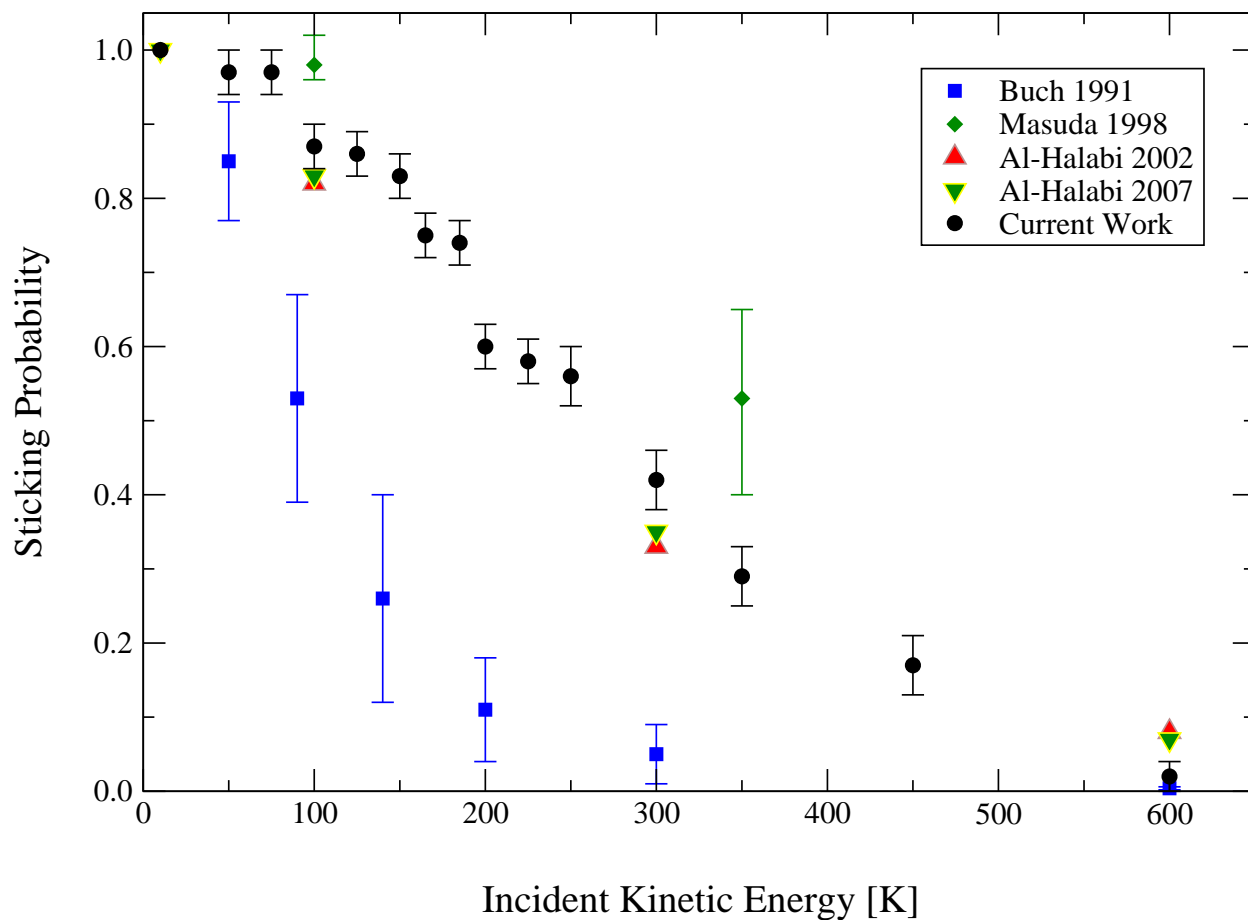


Figure 3.1: Sticking probability vs. incident kinetic energy (in K) of H on amorphous water ice at 10 K, compared to the simulations of Zhang et al. (1991), Masuda et al. (1998), and Al-Halabi & van Dishoeck (2007). Results on crystalline ice from Al-Halabi et al. (2002) are shown for comparison.

3.3.1 Amorphous water ice slab at 10 K

Figure 3.1 shows the sticking probability of atomic hydrogen as a function of incident kinetic energy for an amorphous H₂O slab at 10 K. The sticking probability is essentially 1.0 at very low incident kinetic energy (10 K), and then decreases, slowly at first, with increasing incident kinetic energy, approaching zero at the largest incident kinetic energy studied (600 K). These results differ significantly from those of some previous theoretical studies. The sticking probabilities predicted by Buch & Zhang (1991) are systematically lower than those predicted here and rapidly decrease with increasing incident kinetic energy. For example, at an incident energy of 300 K, the sticking probability predicted by Buch & Zhang (1991) is already well below 0.1, while a value of 0.4 is obtained from the current simulations.

In the Masuda et al. (1998) study there are fewer energies to compare, and the predicted sticking in this case are systematically somewhat higher than our results even at energies of 350 K. However, our results agree fairly well with the Al-Halabi & van Dishoeck (2007) study, but the comparison is limited to only three data points. The study of Al-Halabi et al. (2002), which was carried out on a crystalline ice slab rather than an amorphous ice, shows a similar sticking pattern when compared to the current study, although again the comparison is limited to only three data points. We do however expect higher sticking on an amorphous ice as it is porous and has more active surface interaction sites compared to crystalline ice.

3.3.2 Amorphous water ice slab at 70 K

To study the effect of grain temperature on sticking, we simulated atomic hydrogen incident on an amorphous water ice slab of 70 K, and the results are shown in Figure 3.2. The sticking probability for this system is 0.55 ± 0.05 at low incident energy of the H atom (10 K) and decreases with increasing incident energy to 0.2 ± 0.05 at 350 K. We did a calculation at one very high incident energy (600 K) and found a sticking probability of 0.05 ± 0.05 and agrees

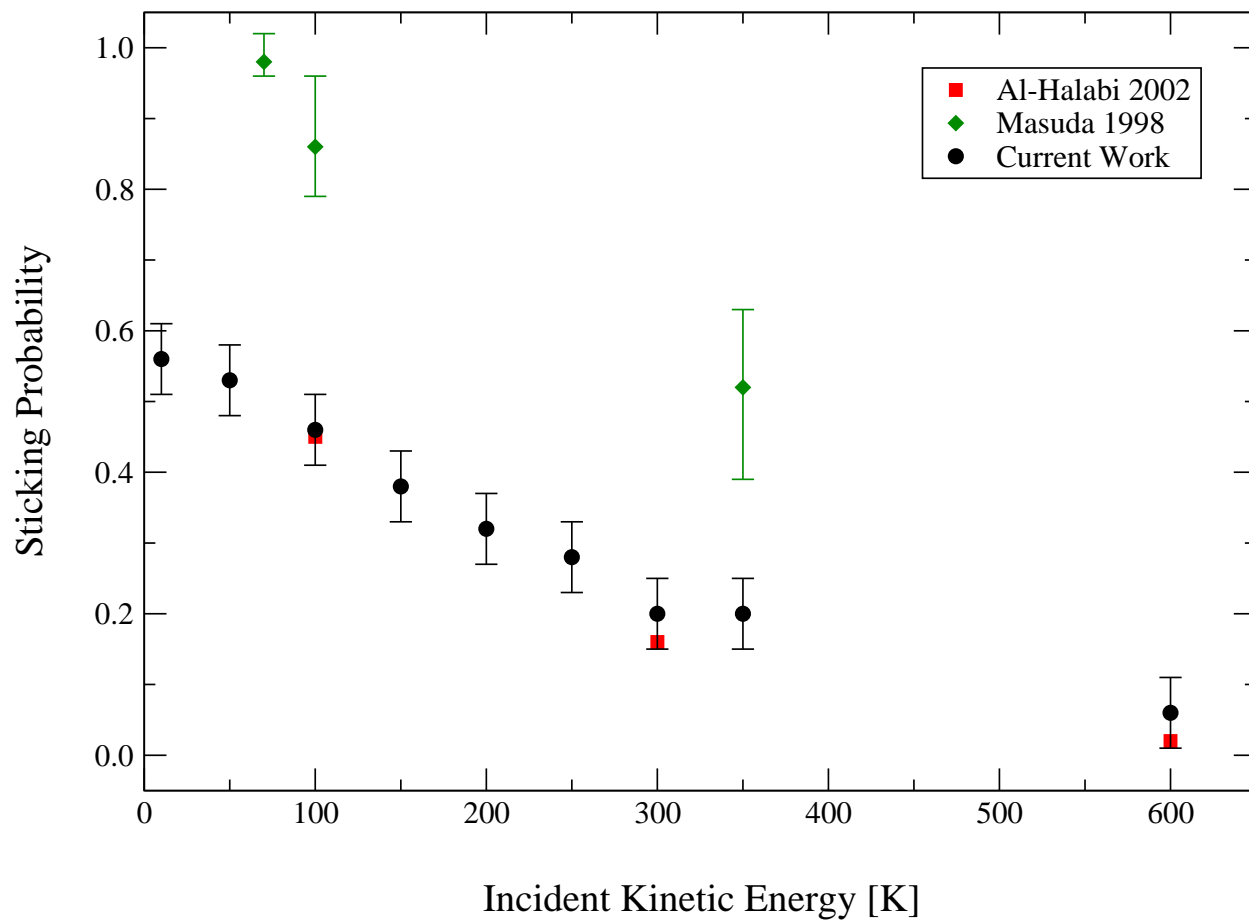


Figure 3.2: Sticking probability of H on amorphous water ice at 70 K, compared to the simulations of Masuda et al. (1998) and Al-Halabi et al. (2002). Note, the results for Al-Halabi et al. (2002) are for crystalline ice.

with the Al-Halabi et al. (2002) result within the error bars. The findings of Masuda et al. (1998) are nearly independent of slab temperatures; they are similar to their 10 K results, and therefore much larger than the current findings. The results of Al-Halabi et al. (2002), while on crystalline ice, are very similar to the current amorphous ice probabilities.

3.3.3 Incident angle of H atom

To study the effect of the incident angle of an impinging hydrogen atom on the sticking probability, we systematically varied the angle from 5° to 85° . The angles were measured from the mean surface of the amorphous ice slab (i.e., normal incidence is at 90°), and for each incident angle 100 trajectories were simulated. The initial (x, y) coordinates of the H atom were selected randomly while keeping the incident kinetic energy and angle fixed.

Figure 3.3 shows the variation of the sticking probability with the angle of incidence. Three different H atom kinetic energies (100 K, 200 K, and 300 K) were considered, and in each case there appears to be a slight trend for the sticking to increase with incident angle. At 300 K, within error bars, the sticking could increase by a factor of 2. As expected, at grazing incidence (close to 0°), there is less probability of sticking compared to angles above 45° , although the effect is small. Hence, we can conclude that the direction of the incident H atom plays only minimal role in sticking. Nevertheless, all our sticking probability calculations (except those in Figure 3.3) include a random sampling over a range of incident angles.

3.4 Discussion

To explain the difference in the sticking probability on ice between the results of Masuda et al. (1998) and Al-Halabi et al. (2002), the latter suggested that incorrect potential parameters were used by Masuda et al. (1998) resulting in higher sticking coefficients. To verify this,

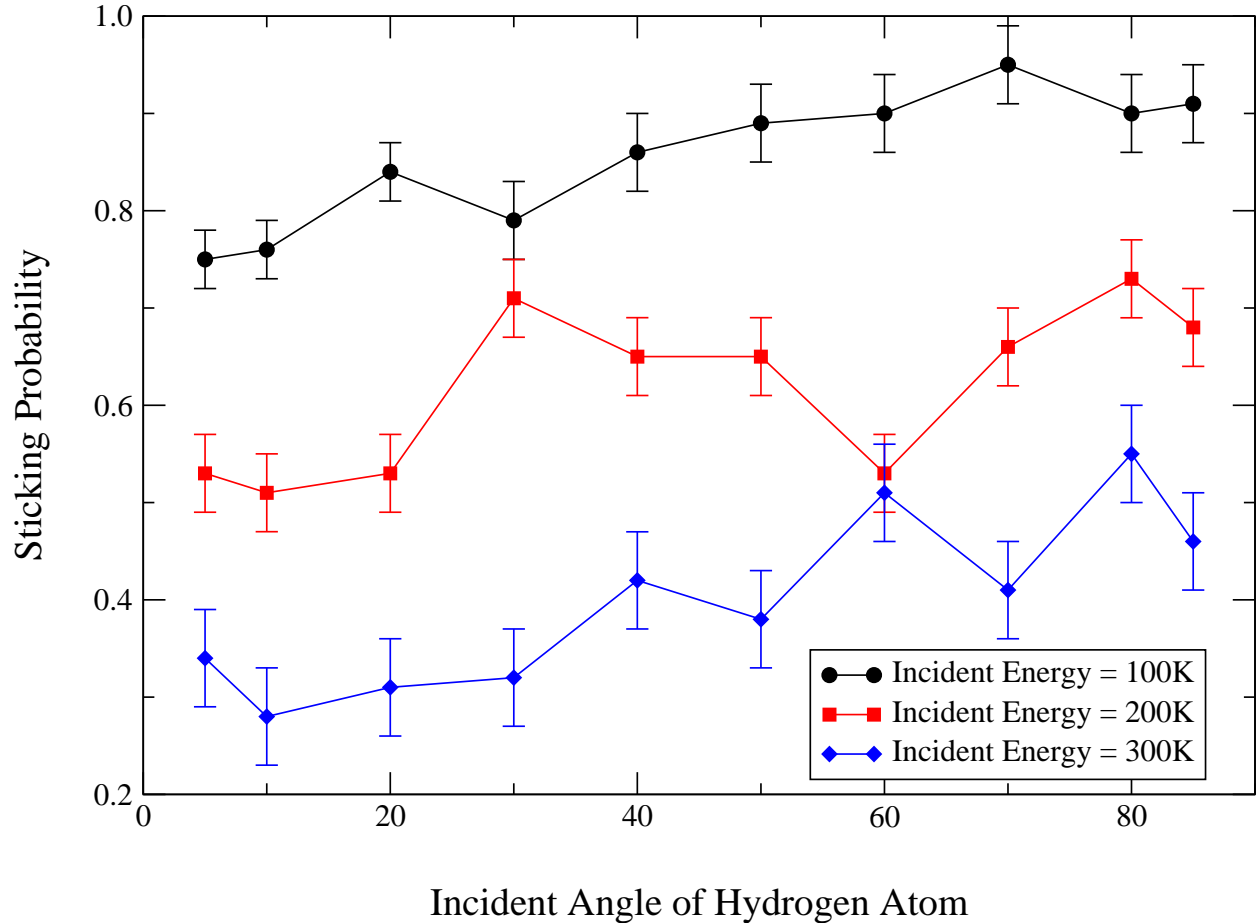


Figure 3.3: Sticking probability as a function of incident angle for three different incident energies. The temperature of the amorphous ice substrate is held at 10 K and normal incidence angle corresponds to 90° .

we adopted the same parameters used by Masuda et al. (1998) and were able to reproduce their results. Following this, we used the corrected potential parameters given by Al-Halabi et al. (2002) for the current simulations. We found a somewhat higher sticking coefficient, compared to Al-Halabi & van Dishoeck (2007), and their results were outside the uncertainty of our simulation results. The results (see Figure 3.2) for crystalline ice of Al-Halabi et al. (2002) are in agreement with the current calculation for amorphous ice at 70 K. The Buch & Zhang (1991) study used 115 water molecules to simulate an amorphous water ice cluster,

with fewer trajectories for each H atom incident kinetic energy. The incident H atom had fewer sites to stick to and less probability of penetrating the ice surface, which we observed to occur in our simulations. This might explain the lower sticking values predicted by their study compared to all other simulations. All the previous studies considered only three to five incident H atom kinetic energies (Figure 3.1); we considered a higher number of incident energies in the current study, up to 350 K (with a few results at higher energy) to gain a better insight into the sticking behavior at different incident energies of the H atom.

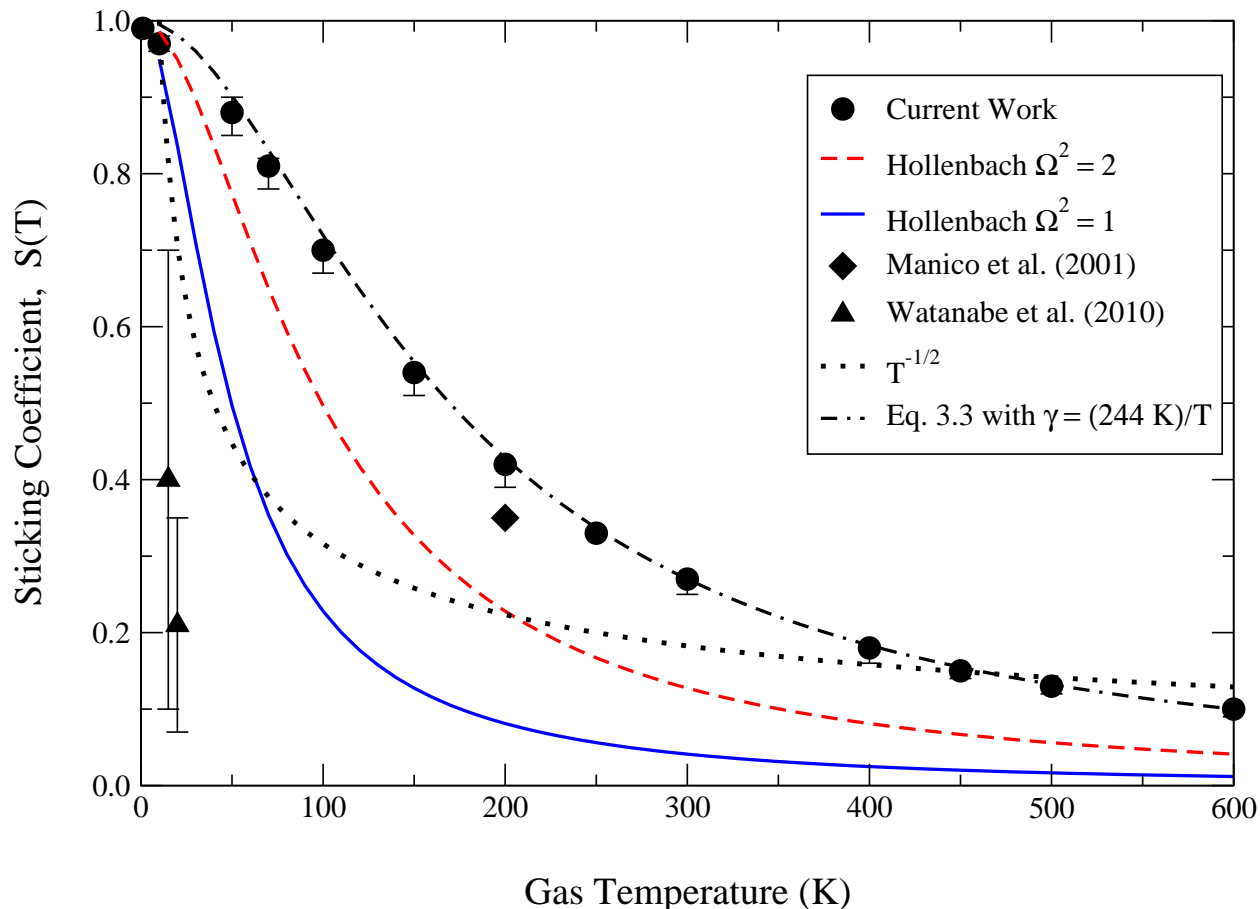


Figure 3.4: Predicted sticking coefficient $S(T)$ of H on 10 K amorphous water ice from the present study compared to the quantum model by Hollenbach & Salpeter (1970) and the experiments of Manico et al. (2001) and Watanabe et al. (2010). Note that the experiments measured $\eta S(T)$ and assume a recombination efficiency, η , of 100%. Also plotted is a $T^{-1/2}$ dependence, normalized to 1 at $T = 10$ K. Fit of current results using Equation (3.3) with $\gamma = (244 \text{ K})/T$.

In Figure 3.4, the sticking coefficients, $S(T)$, from the present study are compared with the theoretical results by Hollenbach & Salpeter (1970) and the experimental data of Manico et al. (2001) and Watanabe et al. (2010). $S(T)$ was obtained by integrating $P(E)$ over a Maxwellian velocity distribution following the approach of Buch & Zhang (1991) for an ice slab of 10 K. The experiment by Manico et al. (2001) reports a parameter Γ , which is the fraction of H atoms that both stick on the surface and eventually form H_2 molecules and leave the surface (i.e., $\Gamma = \eta S(T)$, where η is the probability that an H atom adsorbed on the surface will recombine with another H atom to form H_2 , also known as the recombination efficiency). The authors predicted a sticking probability of 0.4 for a gas temperature of 200 K and for a substrate at 10 K, by assuming the recombination efficiency to be 1. Experiments by Perets et al. (2005) however, showed that the recombination efficiency strongly depends on surface temperature and varies from 0 to 1 over a narrow range (10 K - 14 K). This means that the 0.4 estimated sticking probability is actually a lower limit, with an upper limit at 1.0, depending on the recombination efficiency, η . The study by Watanabe et al. (2010) obtain a sticking coefficient at 15 K and 20 K by assuming a sticking of unity at 8 K. Although they account for loss of H atoms by rapid recombination, they also indicate the possibility of H-atom loss by desorption from the amorphous ice surface. It should be noted that in both these experimental studies, the sticking probability is estimated indirectly from the measured recombination energy of the H_2 molecule formed after the sticking process.

The gas density in the ISM is very low even compared to laboratory vacuum conditions. Meanwhile, the experiments described above used a comparatively high density atom beam, which may lead to surface saturation. This effect may result in a reduced sticking coefficient compared to ISM-like conditions. Hollenbach & Salpeter (1970), in a very general investigation on a crystalline surface, used a lower bound on the H atom binding energy to predict the sticking coefficient. While most studies have shown, an amorphous ice surface has a slightly higher sticking coefficient than a crystalline surface (e.g. Al-Halabi & van Dishoeck (2007)),

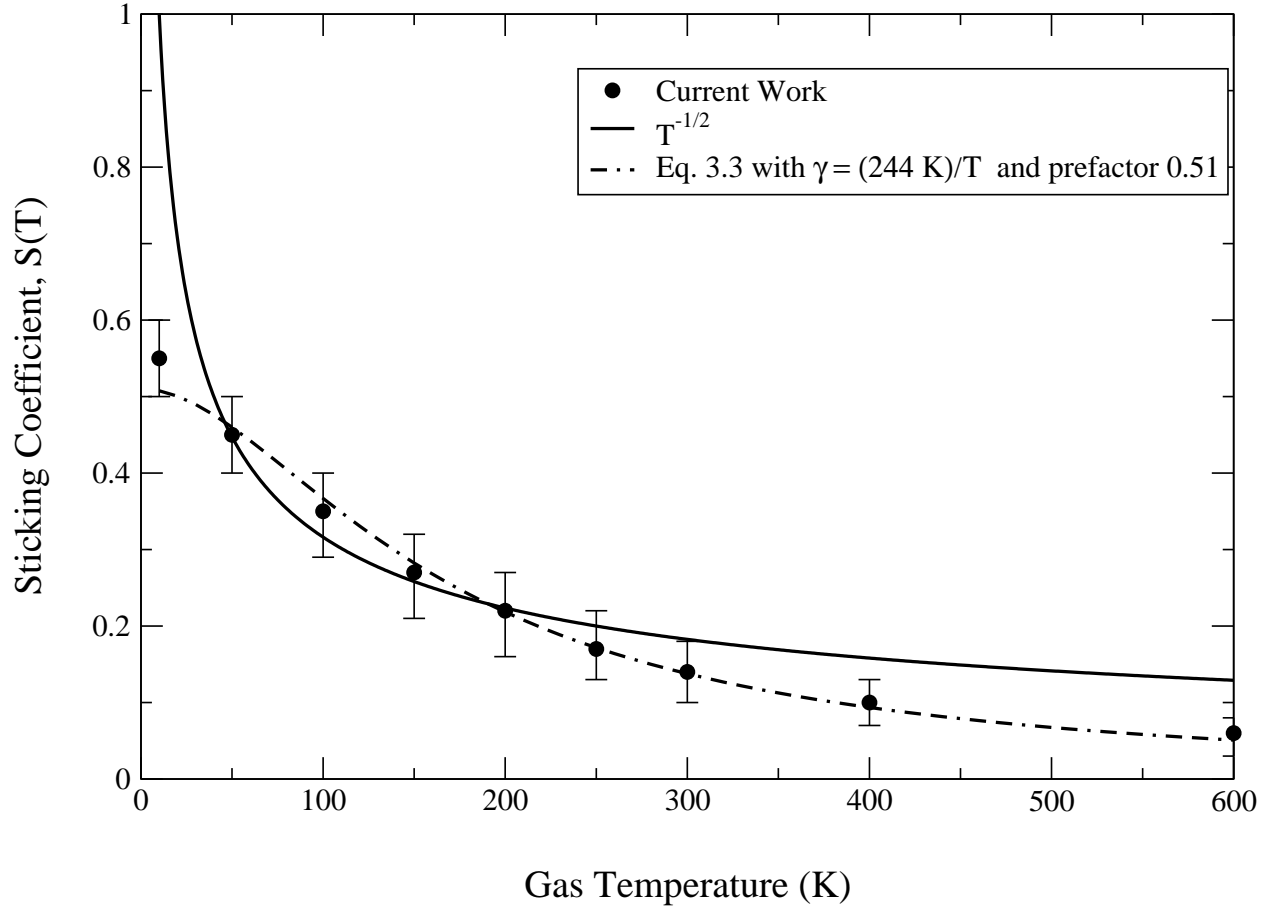


Figure 3.5: Sticking coefficient $S(T)$ of H on 70 K amorphous water ice and fit using Equation (3.3) with $\gamma = (244 \text{ K})/T$ and a prefactor of 0.51. This is compared to $T^{-1/2}$ normalized to 1 at 10K.

the results by Hollenbach & Salpeter (1970) likely underestimate sticking when applied to interstellar conditions. The issues discussed in this paragraph and the last offer possible reasons that experiments report lower sticking coefficients than simulations and theoretical predictions.

The present computational study circumvents some of the theoretical and experimental problems by simulating the conditions in the ISM as closely as possible; i.e., by modeling an amorphous water ice surface and impinging a single hydrogen atom on the surface. We

have also addressed the issues with previous computational studies by correcting the potential parameters, simulating a larger number of trajectories for each incident kinetic energy to reduce statistical errors in estimating the sticking probabilities, and calculating sticking probabilities for a much larger set of incident kinetic energies to enable more precise Maxwellian integration in obtaining $S(T)$ from $P(E)$.

Two issues, however remain for further study. In all simulations that we are aware of to date, the TIP4P water potential was adopted. This is a flexible potential designed primarily for liquid water applications. A more recent potential (Abascal et al., 2005) constructed for solid ice and amorphous water (TIP4P/Ice) may be more suitable, but our preliminary results using the ice potential do not indicate a significant difference in the sticking. For the H-water interaction, a number of potentials have been published since that of Zhang et al. (1991), which was adopted here and all other studies except that of Al-Halabi & van Dishoeck (2007). In that latter study, which used the potential of Andersson et al. (2006), no statistically significant difference was found for the 10 K ice slab compared to their earlier work using the Zhang et al. (1991) potential on amorphous ice. While this surprising result justifies the use of the Zhang et al. (1991) potential for the current work (see also Figure 3.1), further studies using the Andersson et al. (2006) and/or parametrizations of more recent H-water potentials (e.g. Dagdigan & Alexander, 2013) as well as rigid water-water potentials are desirable.

To further aid in astrochemical modeling, we have computed $S(T)$ for the 70 K amorphous ice slab (see Figure 3.5) and obtained non-linear fits to both the 10 and 70 K ice cases. For the fitting, we have adopted the convenient relation obtained by Hollenbach & Salpeter (1970), Equation 3.3, and find $\gamma = (244 \text{ K})/T$ in both cases, but with the overall fit multiplied by pre-factors of 1.0 and 0.51 for 10 and 70 K ice, respectively. The fits, are shown in Figures 3.4 and 3.5, are both consistent with the data and within the estimated uncertainty. Indeed, the fits are excellent.

3.5 Conclusion

The sticking of hydrogen atoms on amorphous ice is an important process for understanding various gas-grain mechanisms in the ISM. This study provides predictions of sticking probabilities for a large number of initial kinetic energies of the H atom and thus gives us a better understanding of the relation between the sticking coefficient and gas temperature. The effect of grain temperature also gives us insight into how the distribution of dust temperatures will eventually effect the sticking probability in the ISM. These results are expected to improve the accuracy of modeling studies of the H₂ formation rate, as the sticking of H has been underestimated in previous work. We find the following relations for the sticking coefficient $S(T_{\text{gas}}, T_{\text{ice}}) = A(\gamma^2 + 0.8\gamma^3)/(1 + 2.4\gamma + \gamma^2 + 0.8\gamma^3)$ where the coefficients are $\gamma = 244/T_{\text{gas}}$ and $A = 1.0$ and 0.51 for $T_{\text{ice}} = 10$ K and 70 K, respectively, which can be used in astrophysical models and further studies involving the sticking of hydrogen on interstellar dust.

Chapter 4

Sticking of Molecular Hydrogen

1

4.1 Introduction

In cold molecular regions of the interstellar medium (ISM), various atomic and molecular species including H, D, C, O, H₂ and CO adsorb on the surface of the icy mantles of dust grains. Further hydrogenation or deuteration of these species at the surface leads to the formation of simple and complex molecules including H₂, CH₄, CH₃OH, and H₂O. Molecules that are formed on the grain surfaces may eventually be returned to the gas phase by reactive desorption, evaporation, photodissociation, cosmic-ray impact, or grain-grain collisions in shocks. These processes are part of gas-grain chemistry, and along with the gas-phase chemistry, describe the formation mechanisms of around 180 molecules found in the ISM and circumstellar envelopes (e.g., Garrod et al., 2008; Millar et al., 1991; Herbst et al., 1997). Atomic and molecular hydrogen are the most abundant species in most astrophysical environments, and the formation mechanism of H₂ in the ISM is a key interstellar process. In

¹This chapter is based on the manuscript Veeraghattam et al. (2014a)

the gas phase, H_2 is primarily formed via the reaction sequence



The shortage of electrons and protons in the ISM, combined with the effects of the incident radiation field destroying H^- before H_2 formation, makes the gas-phase process inefficient (Glover, 2003). The large observed abundance of H_2 cannot be explained by the gas-phase reactions alone. It is well documented that H_2 is primarily formed on grain surfaces in the cold molecular regions of the ISM (see for example Cazaux (2002)).

The sticking of atomic hydrogen on dust grains and subsequent formation of molecular hydrogen has been studied extensively (e.g., Le Bourlot et al., 2012; Iqbal et al., 2012; Takahashi et al., 1999). The sticking coefficient of H atoms on icy mantles, a key parameter in ISM molecular formation models, has also been studied theoretically and experimentally (e.g., Al-Halabi & van Dishoeck, 2007; Watanabe et al., 2010; Veeraghattam et al., 2014), see Chapter 3. As with atomic hydrogen, the interaction of molecular hydrogen with an ice surface and its subsequent sticking or scattering is a key consideration in the formation of various complex molecules in the ISM. While most studies focus on the H_2 formation process itself, there is little understanding of H_2 sticking on ice when incident from the gas phase. There are very few investigations (e.g., Hollenbach & Salpeter, 1970; Leitch-Devlin & Williams, 1985) on molecular hydrogen interactions with ice surfaces in the ISM, with the latter study reported nearly 30 years ago. The quantum mechanical model by Leitch-Devlin & Williams (1985) provides sticking coefficients for H, C, and H_2 on various surfaces (graphite, silicate, and H_2O monolayer on graphite), but has not been used widely in astrophysical models. An experiment by Matar et al. (2010) measured the sticking of H_2 on an amorphous ice surface at 10 K thereby providing the first experimental data on this

topic.

In the ISM, the ortho-para ratio of H_2 is often assumed to be given by the statistical ratio of 3:1 for the populations of the $J = 1$ and $J = 0$ rotational levels or in local thermodynamic equilibrium (LTE) corresponding to the gas kinetic temperature. The actual value of the ratio plays a critical role in the formation and ortho-para ratio of other ions and molecules. For example, the ortho-para ratios of H_3^+ and H_2D^+ (Flower et al., 2006) depend on the ortho-para ratio of H_2 . A number of mechanisms exist to explain ortho-para conversion in the gas phase, such as proton exchange reactions with H^+ and H_3^+ and $\text{H}-\text{H}_2$ collisions. However, in the cold regions of the ISM, gas phase ortho-para reactions are inefficient and cannot explain observed branching ratios. Gas-grain interactions are thus inferred to play an important role in catalyzing the conversion. Ortho-para conversion of H_2 on cold surfaces (10 K graphite) has been observed in laboratory experiments (Palmer & Willis, 1987), and it is suspected that a similar mechanism is at play on the cold dust in the ISM. This process depends on the H_2 sticking coefficient, residence time, and grain temperature (Le Bourlot, 2000), and a fast ortho-para H_2 conversion on cold surfaces has also been suggested. To study the ortho-para conversion process on dust, Le Bourlot (2000) used an assumed sticking coefficient of unity. To this day, many astrophysical models use guessed-at values for the sticking probability (e.g., 0.5 or 1), often with little or no physical basis. Others use the analytical models developed by Hollenbach & Salpeter (1970) and Hollenbach & McKee (1979). The results of the present study indicate that, the former values are rather inadequate, and that a good estimate of the sticking coefficient depends on the incident H_2 gas temperatures.

This chapter reports on an in-depth computational study of H_2 sticking on amorphous ice with the molecular hydrogen in its ground rovibrational state. The grain is modeled as an amorphous ice slab at 10 K, and the sticking probability at a given H_2 kinetic energy is determined from a sequence of simulations of an H_2 molecule impinging the ice slab. Configurational parameters such as incident angle, molecular orientation, and impingement

site are averaged over stochastically. Several incident kinetic energies, ranging from 10 K to 350 K, are considered. Simulations have also been carried at a fixed incident angle of 62° to compare with the experiment of Matar et al. (2010). Following Hollenbach & Salpeter (1970), we use the term “sticking coefficient” to mean a function of gas temperature and the term “sticking probability” to mean a function of incident kinetic energy of the gas molecule. In section 4.2, we describe the simulation methodology and the potential functions used. We present results and discussion in section 4.3 and in section 4.4 provide analysis and a summary.

4.2 Computational Method

To stick to a surface, an impinging atom or molecule must transfer its excess translational energy to the substrate (Zangwill, 1988) or to non-translational molecular excitations. The various dynamical processes involved in this sticking process can be modeled effectively and with minimum bias using classical molecular dynamics (MD). The cold molecular clouds in the interstellar medium, with very low temperatures and pressures, make classical MD a preferred computer simulation method in the area of laboratory astrophysics. In MD, Newton’s equations of motion are integrated numerically to determine the trajectories of each individual atom and/or molecule in a system. The MD simulations presented here have been carried using the Large-scale Atomic/Molecular Massively Parallel Simulator, LAMMPS (Plimpton, 1995). A more detailed introduction to the MD method and the motivation for calculation of sticking coefficient can be found in Chapter 2.

4.2.1 Simulation of Amorphous Ice

In the ISM, dust consists primarily of silicate grains, carbonaceous grains, or a grain covered with multiple layers of amorphous water ice. Observations (Hagen et al., 1981) point to the

existence of water in amorphous ice form in the ISM, and most studies have taken that into account. Grain sizes in diffuse clouds can vary from 0.01 to 60 μm , and a model developed by Weingartner & Draine (2001) suggests that the mass distribution peaks near 0.3 μm . Surface interactions between the adsorbing H_2 and the amorphous water ice result in physisorption, as there is no chemical reaction between the grain and the impinging molecule. All the above conditions need to be taken into account while simulating an ice surface to study the sticking process as described in Section 2.6.

4.2.2 H_2 Interaction with Ice Surface

Using the amorphous water ice slab at 10 K prepared according to section 2.6, we next introduce an H_2 molecule to study the sticking process. The interaction between the hydrogen molecule and the ice surface is calculated using the Zhang & Buch (1992) intermolecular potential for $\text{H}_2\text{-H}_2\text{O}$. In this model, the hydrogen molecule has three charge centers, with each hydrogen atom having a positive charge and the center of the molecular axis having a dummy negative charge. The potential is in the form:

$$V_{\text{H}_2\text{O-H}_2} = \sum_{ij} \frac{q_i q_j}{r_{ij}} + \sum_{k=1}^{k=4} \epsilon_k \left[\left(\frac{\sigma_k}{r_k} \right)^8 - \left(\frac{\sigma_k}{r_k} \right)^6 \right], \quad (4.3)$$

where r_{ij} is the distance between the charge points on H_2O and H_2 . This is a modified Lennard-Jones interaction, and the LJ terms are taken between the center-of-mass of H_2 and the four centers associated with the H_2O molecule: (1) the O atom; (2) and (3) the two H atoms; and (4) the midpoint of the line connecting the two H atoms. The r_{OH} and r_{H_2} bonds are kept rigid. The LJ parameters are listed in Table 1.

k	ϵ [cm^{-1}]	σ [\AA]
1	399.6	3.10
2, 3	179.8	2.15
4	49.9	3.10

Table 4.1: Parameters for the H₂-H₂O interaction potential (Zhang & Buch, 1992).

4.2.3 Sticking Probability

Starting from the vacuum region above the ice slab, a H₂ molecule is launched toward the ice surface with a given initial translational kinetic energy, a random incident angle, a random deposition site, and random initial H₂ molecular bond orientation. The H-H distance is held fixed at the H₂ equilibrium bond length of 0.74 \AA and the initial rotational angular momentum set to zero. For each incident kinetic energy, a minimum of 100 trajectories are simulated for different initial conditions. In the angle resolved study, the incident angle is fixed while the site of deposition and molecular orientation of H₂ axis are chosen randomly. When a H₂ molecule interacts with the ice surface, it either scatters or hops, and then eventually returns to the vacuum or gets stuck on the surface. In the test runs, we ran simulations for a time interval of 20 ps to study the cases of molecules which stick on the surface and we observed that these molecules continued to remain on the surface for the rest of the simulation time. The dependence of sticking on simulation time was studied using the test runs and we found that after 5 ps, the sticking remained constant. The fraction of trajectories that result in the H₂ molecule sticking to the surface gives our estimate of the sticking probability for that incident kinetic energy.

4.2.4 Sticking Coefficient

The sticking coefficient $S(T)$ for incident gas atoms or molecules as defined by Hollenbach & Salpeter (1970) is a function of adsorption or sticking probability, gas temperature, and the fraction of energy transferred in a single collision. An approximation of the analytical form which is used in many astrophysical models is

$$S(T) \approx (\gamma^2 + 0.8\gamma^3)/(1 + 2.4\gamma + \gamma^2 + 0.8\gamma^3), \quad (4.4)$$

and $\gamma = B/T$, where T is temperature and B is constant that depends on the incident atom or molecule species and the type of grain surface.

The estimated sticking probability for a range of incident kinetic energies is used to calculate the sticking coefficient as function of gas temperature via Maxwellian integration,

$$S(T) = \frac{1}{(k_B T)^2} \int_0^\infty P(E) E \exp\left[-\frac{E}{k_B T}\right] dE, \quad (4.5)$$

where $P(E)$ is the sticking probability.

4.3 Results and Discussion

In Figure 4.1, the average sticking probability of H_2 over a range of incident kinetic energies (10–350 K) is shown. For a 10 K ice substrate, the sticking probability has a maximum value of 0.65 and then steadily decreases as the incident energy of the H_2 molecule increases. At incident energies higher than 200 K, the results are as expected, however at low temperatures, the sticking probability is significantly smaller than 1.0. The uncertainty in the sticking probabilities are estimated by randomly sampling from a subset of the trajectories and computing a sticking probability from that sample. The procedure was repeated to obtain a standard deviation, but the reported mean is obtained from the total number of trajectories.

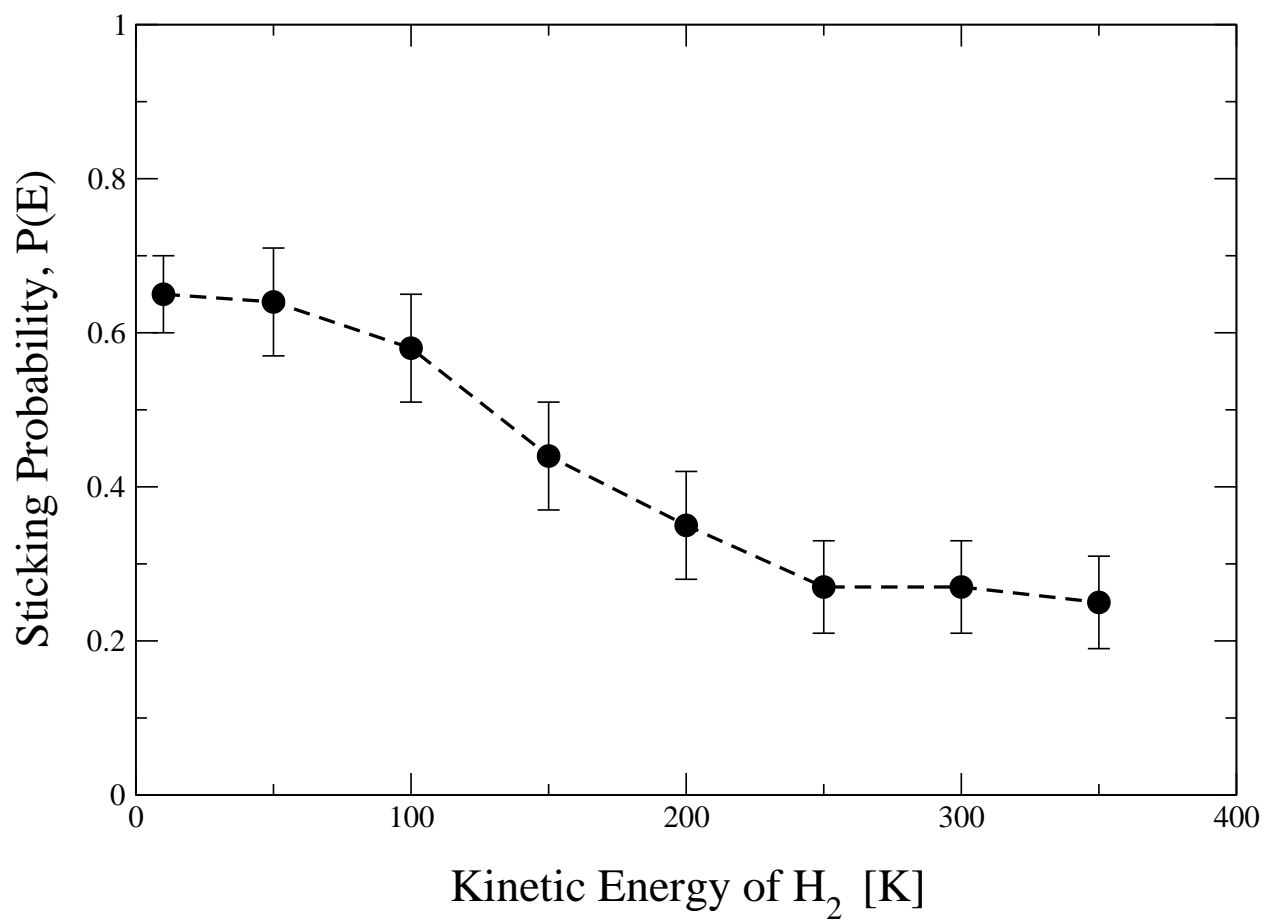


Figure 4.1: Sticking probability vs. incident kinetic energy (in K) of H₂ initially in its ground rovibrational level ($v = 0, J = 0$) on amorphous water ice at 10 K.

In Figure 4.2, the results from previous theoretical studies which calculated the sticking coefficient are compared with the current study. Note that this is a plot of the sticking coefficient as a function of gas temperature, in contrast to the sticking probability as a function of kinetic energy as given in Figure 4.1. This difference is being explicitly stated, as there is some ambiguity in the literature over the terms sticking probability, sticking coefficient, kinetic energy of the atom or molecule, and the gas temperature. The sticking coefficients compared to Hollenbach & Salpeter (1970) and Leitch-Devlin & Williams (1985) show there is a significant variation in predicted values. While Hollenbach & Salpeter (1970) predict a maximum sticking coefficient of 1.0, Leitch-Devlin & Williams (1985) obtain a maximum value around 0.45. Although all three studies follow a similar trend for gas temperatures above 100 K, there is a significant variability at lower gas temperatures. Temperatures below 100 K are of particular interest for cold molecular regions of the ISM, for which the gas is typically 10–20 K, and for the cold neutral clouds, with gas temperatures up to about 100 K.

The theoretical studies mentioned above are very successful in estimating a rough sticking coefficient for a range of molecules and surfaces. Nevertheless, these early pioneering studies made various simplifications and did not adequately simulate surfaces representative of the ISM. Hollenbach & Salpeter (1970) considered a crystalline lattice surface which in turn is a single classical harmonic oscillator with an energy loss function. In contrast, the current investigation used an explicit amorphous surface modeled using 1000 water molecules. In the Leitch-Devlin & Williams (1985) study, lattices are monatomic, i.e., a primitive cell containing only one atom with interaction restricted to nearest neighbors. Also, in their model, when a lattice atom is displaced along one of the principal axes, it gives rise to forces parallel to that axis only. This might be an unrealistic approximation in a H_2 –ice system, where the interaction potential is highly dependent on the directional orientation and thereby effect the sticking.

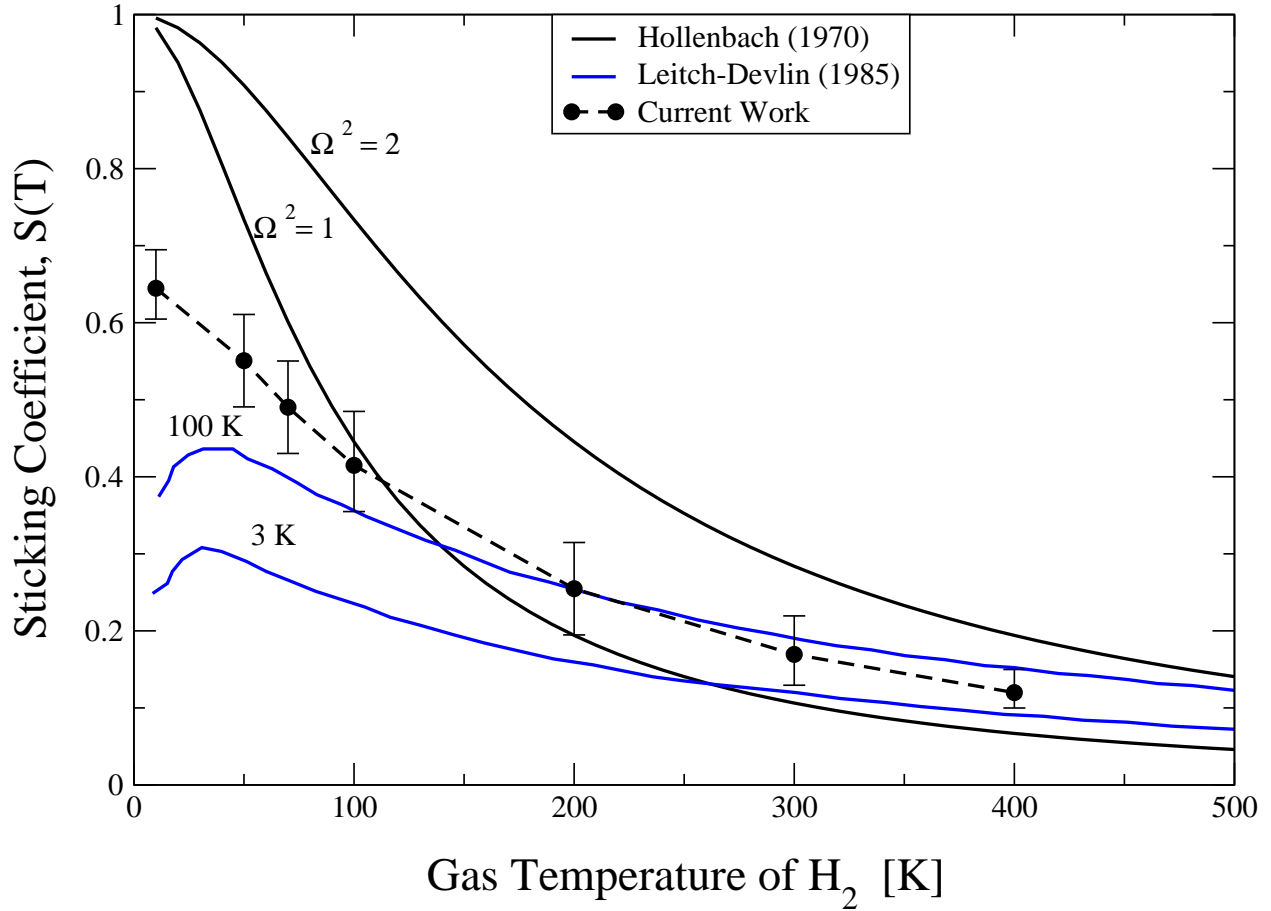


Figure 4.2: Predicted sticking coefficient $S(T)$ of H_2 on 10 K amorphous water ice from the present study compared to the semi-quantum model by Hollenbach & Salpeter (1970) for the two values of the parameter Ω , where $\Omega^2 = 1$ for Lambert's law and $\Omega^2 = 2$ for isotropic scattering. The value of $\Omega^2 = 1$ is typically adopted. Comparison is also made to the quantum mechanical model of Leitch-Devlin & Williams (1985) available only for ice surfaces of 3 and 100 K.

As a test of the current MD approach, our results can be compared to the recent experiment by Matar et al. (2010), which used a molecular hydrogen beam to study sticking on ice surfaces. In the experiment, the angle of incidence of the H₂ beam was set to 62° and the amorphous ice substrate was held at 10 K. The beam energy was varied from 10 K to 350 K and the effective sticking probability measured. To compare the results from the current study, we carried out a sequence of simulation runs in which the incident angle of the H₂ molecules is fixed at 62° and have computed the corresponding sticking probability as a function of H₂ kinetic energy. To directly compare with the measurement, we calculated the effective sticking probability by averaging our computed sticking probability over the velocity spread of the experimental beams as deduced by Matar et al. (2010). Figure 4.3, demonstrates that the current MD approach reproduces the experiment over the kinetic energy range of the measurement. Further, the experiment of Matar et al. (2010) confirms that the sticking probability at low temperatures approaches ~ 0.7 , significantly below 1.

A fit for Equation 4.4, using the results from the current study is given as $S(T_{gas}, T_{ice} = 10K) = 0.63 * (\gamma^2 + 0.8\gamma^3)/(1 + 2.4\gamma + \gamma^2 + 0.8\gamma^3)$, where $\gamma = 226/T_{gas}$. Astrophysical models can use this fit for H₂ sticking coefficients to improve the rate of formation of other molecules and the ortho-para ratio calculations.

The TIP4P water potential and the H₂-H₂O potential by Zhang & Buch (1992) used in this investigations can be improved in further studies. The TIP4P Ice potential by Abascal et al. (2005) might be an improved potential for simulating amorphous water ice surfaces, as this potential has been optimized to simulate solid water and ices, unlike the TIP4P water potential which is optimized for simulating liquid water. A number of studies (e.g., Phillips et al, 1994; Valiron et al., 2008) of the H₂-H₂O system in recent years have provided more accurate potential energy surfaces which could be adopted for use in MD simulations. Including these two changes in the study can increase the accuracy of the sticking probability and coefficients, although the change might not be very significant. Finally, in future studies

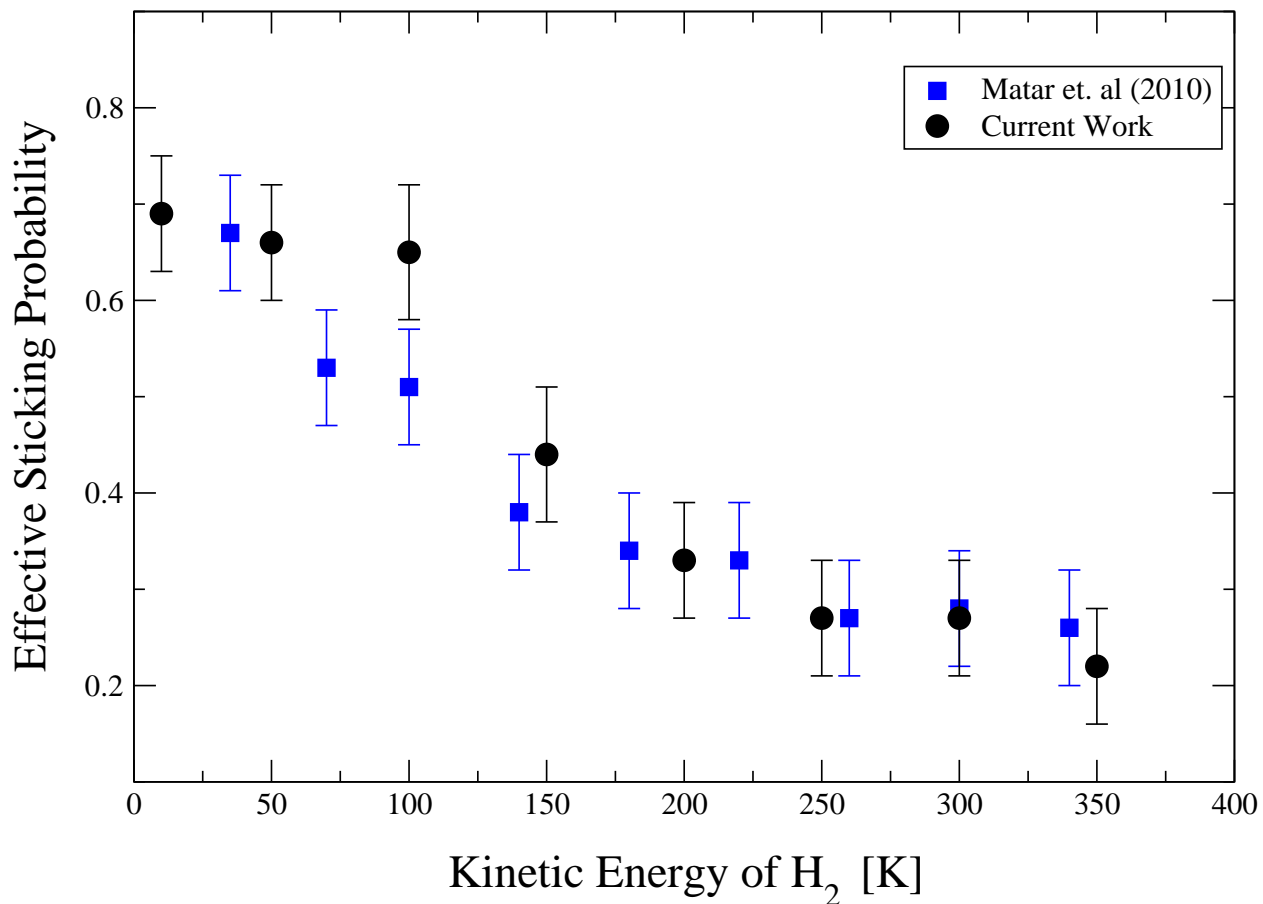


Figure 4.3: Effective sticking probability as a function of H₂ beam kinetic energy (K) on amorphous water ice at 10 K. The computed sticking probability has been averaged over the experimental beam velocity spread for comparison to the experiment of Matar et al. (2010). The angle of incidence is fixed at 62° from the normal.

we hope to explore the effects of varying the initial rovibration state of the incident H_2 by giving the rotor initial angular momentum and allowing for H-H vibrational motion. The later would require adaption of the 9D potential surface of Valiron et al. (2008) which includes vibrational degrees-of-freedom for both partners.

4.4 Conclusion

Using MD simulations, the sticking probabilities of H_2 molecules on the surface of an amorphous water ice at 10 K are calculated. The values of these sticking probabilities agree with the latest experimental results at low and high incident energies of the incident H_2 molecule. The calculated sticking coefficients are an improvement upon the lattice models of Leitch-Devlin & Williams (1985) and provide data to enable improved modeling of the ortho–para ratio of H_2 in molecular regions of ISM. The sticking coefficients will also be applicable for chemical reactions of molecular hydrogen with other chemi- or physisorbed species on grain surfaces.

Further investigations using improved ice and $\text{H}_2\text{-H}_2\text{O}$ potential energy surfaces are desirable. However, the current simulations clearly suggest that often-adopted constant values (e.g. 1 or 0.5) for the sticking coefficients is a rather poor approximation, and the fit provided in this study is a value based on physical processes which is better suited astrophysical models.

Chapter 5

Conclusion

5.1 Summary

The goal of this dissertation has been to simulate the sticking process of atomic and molecular hydrogen on amorphous ice surfaces in order to predict the sticking probability and its dependence on system conditions. The formation mechanism of molecules in the ISM via gas-grain process involves adsorption of an atom or a molecule on the surface. The subsequent formation of a molecule depends on the sticking coefficient of the adsorbing species and hence a crucial factor in the formation rate of molecules including H_2 . Atomic and molecular hydrogen are the two most important species in the ISM and the universe. Understanding the various processes they undergo, and their formation mechanisms are pivotal in gaining a better insight into the evolution of our galaxy. Investigating the sticking probability of H and H_2 on dust surfaces in the ISM has been the core focus of my dissertation.

I have fruitfully used the classical MD technique to simulate the various physical processes that occur when an atom or molecule interacts with an amorphous ice surface. These simulations have incorporated many of the diverse configurational and dynamical features present in the native environment, including random target surface site, random incident

angle, random initial molecular orientation, substrate thermal motion, molecular surface scattering, and of course, molecular sticking.

The sticking probability (a function of incident energy) was determined for substrate temperatures of 10 K (Figure 3.1) and 70 K (Figure 3.2) for a range of incident H energies. The sticking coefficient (a function of gas temperature) was then calculated via Maxwellian integration of the sticking probability and compared to previous experimental and theoretical studies (Figure 3.4). Similarly, for the H₂-ice system, the sticking probability for a substrate temperature of 10 K (Figure 4.1) and a range of incident H₂ energies were obtained from a sequence of independent simulations. The sticking coefficient was then calculated and compared with previous studies (Figure 4.2).

The sticking probabilities and coefficients reported in this work can be used immediately in the astrophysical models to gain a better understanding of the grain-mediated formation mechanism of interstellar species. The various fit parameters I provided are for a widely used analytical model $S(T_{gas}, T_{ice}) = A * (\gamma^2 + 0.8\gamma^3) / (1 + 2.4\gamma + \gamma^2 + 0.8\gamma^3)$, where $\gamma = B/T_{gas}$. and should be easy to incorporate into existing codes. In the Table 5.1, these fit values are summarized.

Species	T _{ice}	A	B
H	10 K	1.00	244
H	70 K	0.51	244
H ₂	10 K	0.63	226

Table 5.1: Fit parameters for the Hollenbach & Salpeter (1970) model

5.2 Future Work

Grain-mediated astrophysical and astrochemical processes are hardly unique to H and H₂. Indeed much contemporary research demonstrates the ubiquitousness of these processes in the ISM, and a host of other atoms and molecules (e.g., C, CO, HD) play important roles. Astrophysical models need reliable, detailed sticking functions in order to incorporate gas-grain phenomena accurately. I am continuing to contribute to that effort through a current, ongoing study of O-atom sticking on amorphous ice. In my future work, I plan to extend these simulation studies to other ISM molecules.

In addition to varying the gas species, I would also like to further investigate the sticking process for a range of dust temperatures and grain types (e.g., silicates, graphites), to better understand its role in gas-grain phenomena. In this dissertation, I studied the sticking as a function of incident kinetic energy and two different ice temperatures. The astrophysical community would benefit from a sticking function which is a function of both gas and dust temperature, and by studying the sticking process over a range of ice temperatures, we can provide $S(T_{gas}, T_{dust})$. This will in turn enable the modelers to make accurate calculations of the formation rate of various species in the ISM and better understand how the microphysical processes effect the evolution of the universe.

Bibliography

- Abascal, J.L.F., Sanz, E., Fernandez, R.G., & Vega C. 2005, *J. Chem. Phys.* 122, 234511
- Al-Halabi, A., Kleyn, A. W., van Dishoeck, E. F., & Kroes, G. J. 2002, *J. Phys. Chem., B* 106, 6515
- Al-Halabi, A. & van Dishoeck, E.F. 2007, *MNRAS*, 382, 1648
- Allen, M. P. & Tildesley, D. J. 1987, *Computer Simulation of Liquids* (Clarendon Press, Oxford)
- Andersson, S., Al-Halabi, A., Kroes, G., & van Dishoeck, E. F., 2006, *J. Chem. Phys.*, 124, 064715
- Buch, V. & Zhang, Q., 1991, *ApJ*, 379, 647
- Cazaux, S., & Tielens, A., G., G., M. 2002, *ApJ*, 575, L29
- Cazaux, S., Morisset, S., Spaans, M., & Allouche, A. 2011 *A&A*, 535, A27
- Cunha, E., Charlot, S., & Elbaz, D. 2005, *MNRAS*, 388,1595
- Cuppen, H. M., Kristensen, L. E., & Gavardi E. 2010, *MNRAS*, 406, L11
- Dagdigian, P.J., & Alexander, M.H. 2013, *J. Chem. Phys.*, 139, 194309
- Draine, B. T. 2003, *Annual Review of Astronomy & Astrophysics*, 41, 241

Eley D. D. 1941, Proc. R. Soc. London, 178, 452

Garrod, R. T., Widicus-Weaver, S. L., & Herbst, E. 2008, ApJ, 628, 283

Ewald, P. 1921, Ann. Phys. 64, 253

Flower, D.R., Pineau des Forets, G., & Walmsley C.M. 2006, A&A, 449, 621

Glover, C.O. Simon 2003, ApJ, 548, 331

Gould, R. J. & Salpeter, E. E. 1963, ApJ, 138, 393

Hagen, W., Tielens, A.G.G.M., & Greenberg, J.M. 1981, Chem. Phys., 56, 367

Harris, J. & Kasimo, B. 1981, Surf. Sci., 105, L281

Heiles, C. & Troland, T. M. 2004, ApJS, 151, 27

Herbst, E., Green, S., Thaddeus, P., & Klemperer, W. 1977, ApJ, 215, 503

Hinshelwood, C. N. 1930, Ann. Res. London Chem. Soc., 27, 11

Hoover, W. G. 1985, Phys. Rev. A., 31, 1695

Hollenbach, D., Kaufman, M. J., Bergin, E. A., & Melnick G. J. 2009, ApJ, 690,1497

Hollenbach, D. & McKee, C. F. 1979, ApJS, 41, 555

Hollenbach, D., & Salpeter, E. E. 1971, ApJ, 163 155

Hollenback, D. & Salpeter, E. E. 1970, J. Chem. Phys., 53, 79

Hornekær, L., Baurichter, L., Petrunin, V. V., Field, D., & Luntz, A. C. 2003, Science, 302, 1943

Iqbal, W., Acharya, K., & Herbst, E. 2012, ApJ, 751, 58

- Jorgenson, W. L. 1982, J. Chem. Phys., 77, 4156
- Kroes, G. J. & Clary, D. C. 1992, J. Phys. Chem., 96, 2682
- Landau, D. P., & Binder, K., 2000, *A Guide to Monte-Carlo Simulations in Statistical Physics*, Cambridge University Press.
- Langmuir, I. 1922, Trans. Faraday Soc., 17, 621
- Le Bourlot, J., Pineau des Forets, G., Roueff, E., & Flower, D. R. 1995b, A&A, 302, 870
- Le Bourlot, J. 2000, A&A. 360, 656
- Le Bourlot, J. , Petit, F. Le, Pinto, C., Roueff, E. & Roy F. 2012, A&A, 541, A76
- Leitch-Devlin, M. A. & Williams, D. A. 1985, MNRAS, 213, 295
- Lennard-Jones, J. E., & Devonshire, A. F. 1936, Nature, 137, 1069
- Lepp, S., Stancil, P. C., & Dalgarno, A. 2002, Atomic and Molecular Processes in the Early Universe, J. Phys. B, 35, R57
- Manico, G., Raguni, G., Pirronello, V., Roser, J.E., & Vidali, G. 2001, ApJ, 548, L253
- Matar, E., Bergeron, H., Dulieu, F., Chaabouni, H., Accolla, M. & Lemaire J. L. 2010, J. Chem. Phys., 133, 104507
- Mathis, J. S., Rumpl, W. & Nordsieck, K.H. 1977, ApJ, 217, 425
- Masuda K., Takahashi J., & Mukai, T. 1998, A&A, 330, 773
- Millar, T. J., Herbst, E., & Charnley, S. B. 1991, ApJ, 369, 147
- Müller, H. S. P., Schlöder, F., Jürgen, S., Winnewisser, G. 2005, J. Mol. Structure, 742, 215
- Nosé, S. 1984, J. Chem. Phys., 8, 511

- Palmer, R.E., & Willis, R.F. 1987, Surf. Sc. 179, L1
- Perets, H. B., Biham O., Manico, G., Pirronello, V., Roser, J., Swords, S., & Vidali, G. 2005, ApJ, 627, 850
- Phillips, T.R., Maluendes, S., McLean, A. D., & Green, S. 1994, J. Chem. Phys., 101, 5824
- Plimpton, S. 1995, J. Comp. Phys., 117, 1 (<http://lammps.sandia.gov>)
- Rappaport, D. C., 2004, *The Art of Molecular Dynamics Simulation*, Cambridge University Press.
- Ryckaert, J.P., Ciccotti, G., & Berendsen, H.J.C. 1977, J. Comp. Phys. 23(3), 327
- Saslaw, W. C. & Zipoy, D. 1967, Nature, 216, 976
- Stancil, P.C., Schultz, D.R., Kimura, K., Gu, J.P., & Buenker, R.J. 1999, Aston. Astrophys. Suppl. Ser., 140, 2, 225
- Takahashi, J., Masuda, K. & Nagaoka, M.1999, MNRAS, 306, 22
- Tielens, A. G. G. M. 2005, *The Physics and Chemistry of the Interstellar Medium*, Cambridge University Press.
- Valiron, P., Wernli, M., Faure, A., Wiensfeld, L., Rist, C., Kedzuch, S., & Noga, J. 2008, J. Chem. Phys., 129, 134306
- Veeraghattam, V. K., Manrodt, K., Lewis, S. P., & Stancil, P. C. 2014, ApJ, 790, 4
- Veeraghattam, V. K., Lewis, S. P., & Stancil, P. C. 2014, ApJ (manuscript)
- Verlet, L. 1967, Phys. Rev. 159, 98
- Watanabe, N., Kimura, Y., Kouchi, A., Chigai, T., Tetsuya, H., & Pirronello, V. 2010, ApJ, 714, L233

Weingartner, J. C. & Draine, B. T. 2001, *ApJ*, 548, 296

Zangwill, A. 1988, *Physics at Surfaces* (Cambridge Press, Cambridge)

Zhang, Q., Sabelli, N., & Buch V. 1991, *J. Chem. Phys.*, 95, 1080

Zhang, Q., Szczesniak, M. M., & Buch V. 1992, *J. Chem. Phys.*, 96, 6039